PREPARED FOR THE U.S. DEPARTMENT OF ENERGY,
UNDER CONTRACT DE-AC02-76-CHO-3073

PPPL-3093
UC-427

PPPL-3093

TRAPPED ION MODE IN TOROIDALLY ROTATING PLASMAS

BY

M. ARTUN, W.M. TANG AND G. REWOLDT

APRIL 1995

PRINCETON
PLASMA PHYSICS
LABORATORY

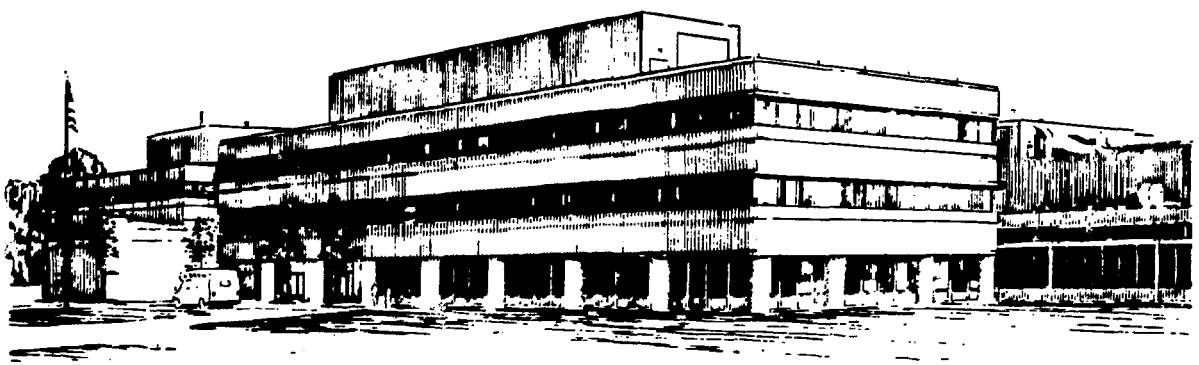

PRINCETON UNIVERSITY, PRINCETON, NEW JERSEY

NOTICE

NOTICE

Trapped Ion Mode in Toroidally Rotating Plasmas

M. Artun*, W. M. Tang, and G. Rewoldt

Princeton University Plasma Physics Laboratory

P. O. Box 451

Princeton, NJ 08543-0451

Abstract

The influence of radially sheared toroidal flows on the Trapped Ion Mode (TIM) is investigated using a two-dimensional eigenmode code. These radially extended toroidal microinstabilities could significantly influence the interpretation of confinement scaling trends and associated fluctuation properties observed in recent tokamak experiments. In the present analysis, the electrostatic drift kinetic equation is obtained from the general nonlinear gyrokinetic equation in rotating plasmas [M. Artun and W. M. Tang, Phys. Plasmas, 1 2682 (1994)]. In the long perpendicular wavelength limit $k_\tau \rho_{bi} \ll 1$, where ρ_{bi} is the average trapped-ion banana width, the resulting eigenmode equation becomes a coupled system of second order differential equations for the poloidal harmonics. These equations are solved using finite element methods. Numerical results from the analysis of low and medium toroidal mode number instabilities are presented using representative TFTR L-mode input parameters. To illustrate the effects of mode coupling, a case is presented where the poloidal mode

*Present address: University of California, Los Angeles, Department of Physics, Los Angeles, CA 90024-1547

coupling is suppressed. The influence of toroidal rotation on a TFTR L-mode shot is also analyzed by including a beam species with considerable larger temperature. A discussion of the numerical results is presented.

I. Introduction

The influence of sheared equilibrium flows on tokamak microinstabilities is a topic of considerable importance to the fusion community. Experimental evidence as well as theoretical studies indicate that radially sheared equilibrium flows have a favorable impact on the energy transport associated with low frequency electrostatic microturbulence.

In the magnetic braking experiments performed on DIII-D, LaHaye, *et al.*[1] have observed that when core toroidal rotation was reduced by applying magnetic braking in the Very High (VH) confinement mode, the ion heat conductivity χ_i increased significantly with only minor changes in temperature and density profiles. Fluctuation measurements on TFTR by Fonck, *et al.*[2] indicate that the radial correlation length decreases significantly as core toroidal rotation is increased.

Theoretical studies of the kinetic Ion Temperature Gradient (ITG) instability in the simplified sheared slab geometry have generally found a strong reduction in the linear growth rate in the presence of radially sheared perpendicular flows. It was concluded that the mode is stabilized by perpendicular sheared flows with magnitudes of the order $v_\perp \sim \mathcal{O}(\sqrt{\rho_i/L_T}v_{ti})$ and a shear length comparable to other equilibrium scale lengths in the system, $L_{v_\perp} \sim \mathcal{O}(L_T)$. However, the extrapolation of this result to full toroidal geometry is not straightforward. Even though toroidal effects such as curvature and ∇B drifts are incorporated in various semi-slab studies, a proper kinetic treatment of trapped particles requires a fully two-dimensional analysis in toroidal geometry. The most prominent type of long wavelength toroidal microinstabilities is the trapped-ion mode (TIM) in the presence of a significant ion temperature gradient. One of the most important feature of these instabilities is their global nature, *i.e.*,

large radial correlation lengths that can vary on the equilibrium (*i.e.*, toroidal minor radius) scale length rather than on the ion gyroradius scale length usually associated with kinetic microinstabilities. Heuristic estimates of energy transport make these the leading candidates to account for the Bohm-like confinement observed in many experiments.

In this paper, we perform the first eigenmode analysis of the influence of sheared toroidal rotation on the trapped-ion mode in a low-β tokamak. The initial work by Kadomtsev *et al.*[3] indicates that the TIM has a real frequency below the diamagnetic drift frequency, ω_{*i}, and below the bounce frequency ω_{bi}. These instabilities are easier to excite in the core region of tokamak fusion plasmas where the plasma can be considered to be effectively collisionless. For typical fusion plasma parameters in the core region, both the diamagnetic drift frequency and the ion bounce frequency are well above the ion-ion collision frequency. Hence, for the time scales of interest, collisions are not expected to have a significant effect. Collisional effects on the trapped-ion mode[4] and the sheared slab ion temperature gradient mode have been treated elsewhere[5] and will not be considered in our analysis.

To facilitate the analysis of the problem a few simplifying assumptions are made. The mode is considered to be purely electrostatic due to low plasma pressure, *i.e.*, low β, and the magnetic surfaces are taken to be concentric circles. Considering low toroidal mode numbers, the radial wavenumber, k_r, is assumed to be small, satisfying $k_r \rho_{bi} \lesssim 1$, where ρ_{bi} is the ion banana width. Under these assumptions, finite larmor radius effects can be ignored since $\rho_i/\rho_{bi} \sim \mathcal{O}(\epsilon^{1/2}/q)$. This justifies using the electrostatic drift kinetic equation. Integrating along unperturbed particle orbits leads to the perturbed distribution function, and the quasineutrality condition is then used to close the system of equations. The resulting set of eigenmode equations is solved using finite element methods.

The equilibrium parameters studied in this paper are taken from the TFTR L-mode shot #49982. Results from calculations with full poloidal mode coupling as well as cases where mode coupling is artificially suppressed, are presented. The effect

of hot particles is also analyzed for this type of discharge since a beam species with significantly higher temperature and small density fraction is present. It can be argued that since these particles have much larger thermal speeds, the toroidal rotation of the main ion population should not be felt by these particles and toroidal rotation stabilization would thereby not be as significant in the presence of beam species.

The rest of this paper is organized as follows. In Sec. II the drift kinetic equation is presented and equilibrium quantities in the presence of toroidal rotation are described. Sec. III describes the derivation of the two-dimensional eigenmode equation based on the earlier derivation by Marchand.[6,7] In Sec. IV numerical results are presented followed by a summary and discussion of results in Sec. V.

II. Kinetic Equations and Equilibrium

The drift kinetic equation used in the analysis of the trapped ion mode to calculate effects of sheared toroidal rotation is obtained by taking the linear electrostatic limit of the general geometry nonlinear gyrokinetic equations derived by Artun and Tang[8] in the presence of axisymmetric plasma rotation. This derivation involves transforming the velocity variable to the moving frame. The new velocity variable is defined as $\mathbf{c} \equiv \mathbf{v} + \mathbf{V}$, where $\mathbf{V}$ is the toroidal rotation velocity assumed to be of the form $\mathbf{V} = \Omega(\psi) R \hat{\boldsymbol{\zeta}}$. Here ψ is the poloidal magnetic flux, R is major radius, and $\hat{\boldsymbol{\zeta}}$ is the unit vector in the toroidal direction.

Considering modes with $k_r \rho_{bi} \lesssim 1$ implies $k_\perp \rho_i \ll 1$ for large aspect ratio (or large q) tokamaks. In the limit

$$\lim_{k_\perp \rho_i \to 0} J_0(k_\perp \rho_i) = 1,$$

the gyrokinetic equation becomes the drift kinetic equation:

$$\left[\frac{\partial}{\partial t} + \left(c_\parallel \hat{\mathbf{n}} + \mathbf{V} + \mathbf{c}_\mathrm{D}\right) \cdot \boldsymbol{\nabla}\right] h = -Ze \frac{\partial F}{\partial E} \Bigg(\left[\frac{\partial}{\partial t} + \mathbf{V} \cdot \boldsymbol{\nabla}\right] \Phi \tag{1}$$

$$+ \frac{1}{\Omega_c} \left[\boldsymbol{\nabla}\Phi \times \hat{\mathbf{n}} \cdot \boldsymbol{\nabla}\mathbf{V} \cdot (c_\parallel \hat{\mathbf{n}} + \mathbf{V}) + (c_\parallel \hat{\mathbf{n}} + \mathbf{V}) \cdot \boldsymbol{\nabla}\mathbf{V} \cdot \boldsymbol{\nabla}\Phi \times \hat{\mathbf{n}}\right] \Bigg) \tag{2}$$

$$+\frac{Ze}{M}\frac{1}{\Omega_c}\nabla\Phi\times\hat{\mathbf{n}}\cdot\nabla F. \tag{3}$$

Here h is the non-adiabatic portion of the perturbed distribution function given by

$$f = h + Ze\Phi\frac{\partial F}{\partial E}. \tag{4}$$

Φ is the perturbed electrostatic potential, and $\hat{\mathbf{n}}$ is the unit vector along the magnetic field. The equilibrium electrostatic potential Φ_0 is what remains after the lowest order electrostatic potential, Φ_{-1}, which is necessary for radial force balance, has been transformed away.[8]

The guiding center drift velocity, $\mathbf{c}_D$, with the Coriolis and centrifugal forces taken into account, is

$$\mathbf{c}_D = \frac{\hat{\mathbf{n}}}{\Omega_c}\times\left[\frac{Ze}{M}\nabla\Phi_0 + \frac{c_\perp^2}{2}\nabla\ln B + (c_\parallel\hat{\mathbf{n}} + \mathbf{V})\cdot(\nabla\mathbf{V} + c_\parallel\nabla\hat{\mathbf{n}})\right], \tag{5}$$

and F is the equilibrium distribution function, which is assumed to be an isotropic Maxwellian in the energy variable, E. The lowest order expressions for the guiding center variables are:

$$E = \frac{Mc_\parallel^2}{2} + \mu B - \frac{M\Omega^2R^2}{2} + Ze\Phi_0, \tag{6}$$

$$\mu = \frac{Mc_\perp^2}{2B}, \tag{7}$$

$$\text{and}\quad \mathbf{R} = \mathbf{x} + \frac{\mathbf{c}_\perp\times\hat{\mathbf{n}}}{\Omega_c}, \tag{8}$$

where Ω is the angular rotation frequency which must be a flux function to satisfy equilibrium constraints,[9] and $\Omega_c \equiv ZeB/Mc$ is the Larmor frequency.

II.A Equilibrium Electrostatic Potential

In the derivation of the general gyrokinetic equation, it was indicated that the equilibrium distribution function had to be of the form[8]

$$F = F(\mathbf{R}_\perp, \mu, E). \tag{9}$$

Hence for an isotropic Maxwellian distribution function ($\partial/\partial\mu = 0$) in circular toroidal geometry, we have:

$$F = \bar{n}(r)\frac{1}{\pi^{3/2}v_{th}^3}\exp[-E/T] \tag{10}$$

where $\bar{n}(r)$ is a flux function related to density. Using the Jacobian for the velocity space variables in the rotating and laboratory frames,

$$\left|\frac{\partial \mathbf{c}}{\partial \mathbf{v}}\right| = 1, \tag{11}$$

one can easily integrate the perturbed distribution function to obtain the following expression for the density:

$$n = \bar{n}(r)\exp\left[\frac{M\Omega^2R^2}{2T} - \frac{Ze\Phi_0}{T}\right]. \tag{12}$$

However, this expression yields different densities for ions and electrons at different poloidal locations for an arbitrary choice of the equilibrium potential Φ_0. The main reason is that the centrifugal forces experienced by the ions and electrons are vastly different, and the force experienced by the electrons is negligible for all practical purposes. The large centrifugal force on the ions is reduced by this electrostatic potential and at the same time the electrons are pulled into the ions in order to maintain quasineutrality. Hence, equilibrium can only be achieved by the appropriate choice of Φ_0. To incorporate the poloidal variation, one can assume $\Phi_0 \sim R^2$, *i.e.*,

$$\Phi_0(r,\theta) = \bar{\Phi}_0(r)\frac{R^2(r,\theta)}{R_0^2}. \tag{13}$$

An expression for Φ_0 can be obtained by making a large aspect ratio expansion of R. Expanding $R^2 \simeq R_0^2(1 + 2\epsilon\cos\theta)$ to first order in $\epsilon \equiv r/R_0$, one can define:

$$n_0(r) = \bar{n}(r)\exp[\frac{M\Omega^2 R_0^2}{2T} - \frac{Ze\bar{\Phi}_0}{T}], \tag{14}$$

to obtain:

$$n = n_0(r)\exp\left[\frac{M\Omega^2 R_0^2}{2T}2\epsilon\cos\theta - \frac{Ze\bar{\Phi}_0}{T}2\epsilon\cos\theta\right]. \tag{15}$$

The quasineutrality condition can now be solved order by order. To lowest order in the expansion parameter ϵ, the quasineutrality condition will be satisfied by the choice of

$$n_{0j} = f_j n_{0e}, \tag{16}$$

and requiring $\sum_{j\neq e} Z_j f_j = 1$, where n_{0e} is the electron density. To next order in ϵ, we expand the exponential in Eq. (15) and the quasineutrality condition becomes:

$$\frac{\Omega^2 R_0^2}{2}\sum_j \frac{Z_j f_j M_j}{T_j} - e\bar{\Phi}_0 \sum_{j\neq e}\frac{Z_j^2 f_j}{T_j} = \frac{e\bar{\Phi}_0}{T_e}, \tag{17}$$

where we have ignored the centrifugal force on electrons. Solving for $\bar{\Phi}_0$ and substituting in Φ_0 we obtain:

$$\Phi_0 = \frac{\Omega^2 R^2}{2e}\left[\frac{1}{T_e} + \sum_{j\neq e}\frac{Z_j^2 f_j}{T_j}\right]^{-1}\sum_{j\neq e}\frac{Z_j f_j M_j}{T_j}. \tag{18}$$

Defining

$$Z_j e\Phi_0 = \alpha_j \frac{M_j\Omega^2 R^2}{2}, \tag{19}$$

with

$$\alpha_j = \frac{Z_j}{M_j}\left[\frac{1}{T_e} + \sum_{k\neq e}\frac{Z_k^2 f_k}{T_k}\right]^{-1}\sum_{k\neq e}\frac{Z_k f_k M_k}{T_k}, \tag{20}$$

the energy for species j will be given by

$$E = \frac{M_j c_\parallel^2}{2} + \frac{\mu B_0}{h(\theta)} - (1-\alpha_j)\frac{M_j \Omega^2 R^2}{2}, \tag{21}$$

where $h(\theta) \equiv 1 + \epsilon \cos\theta$. Ignoring terms of $\mathcal{O}(\epsilon^2)$, it is convenient to define a new energy variable

$$E' = \frac{M_j c_\parallel^2}{2} + \frac{\mu B_0}{h} - 2\epsilon \cos\theta (1-\alpha_j)\frac{M_j \Omega^2 R_0^2}{2} \tag{22}$$

which will only include the poloidally varying part of the centrifugal and electrostatic potential. Since terms of $\mathcal{O}(\epsilon^2)$ have been neglected, it is useful to slightly modify E' (for reasons to become clear later) to obtain:

$$E' = \frac{M_j c_\parallel^2}{2} + \frac{\mu B_0}{h(\theta)} - \frac{\epsilon g_j \cos\theta}{h}, \tag{23}$$

where

$$g_j \equiv 2(1-\alpha_j)\frac{M_j \Omega^2 R_0^2}{2}. \tag{24}$$

Then, using the definition of n_0 introduced above, the equilibrium distribution will be given by:

$$F = F_M(E') = \frac{n_0(r)}{v_{th}^3 \pi^{3/2}} e^{-E'/T}. \tag{25}$$

It is convenient to define the dimensionless variables $\bar{E} \equiv E'/T$, $\bar{\mu} \equiv \mu B_0/T$, and $\bar{g} \equiv g/T$. In terms of these variables the expression for the parallel velocity $c_\parallel$ is given by:

$$h(\theta) c_\parallel^2 = v_{th}^2 (\bar{E} + \bar{g}) \left[\frac{\bar{E} - \bar{\mu}}{\bar{E} + \bar{g}} + \epsilon \cos\theta \right]. \tag{26}$$

We can then define

$$\Lambda \equiv \frac{\bar{\mu} + \bar{g}}{\bar{E} + \bar{g}} \tag{27}$$

such that the expression for the parallel velocity becomes:

$$c_{\|} \simeq \sigma_{\|}\gamma^{1/2}v_{th}\sqrt{1-\frac{\Lambda}{h(\theta)}} \tag{28}$$

with $\gamma \equiv \bar{E} + \bar{g}$. It is useful to note here that γ is the rotation modified energy variable which will appear in most expressions involving particle orbits.

II.B Perturbed Distribution Function

Using the modified energy variable defined in Eq. (22) and using Eqs. (3) and (4), the equation for the perturbed distribution function f becomes:

$$\left(\frac{\partial}{\partial t} + c_{\|}\hat{\mathbf{n}}\cdot\boldsymbol{\nabla} + \mathbf{c}_D\cdot\boldsymbol{\nabla} + \mathbf{V}\cdot\boldsymbol{\nabla}\right) f = -Ze\frac{\partial F}{\partial E'}\left(c_{\|}\hat{\mathbf{n}}\cdot\boldsymbol{\nabla} + \mathbf{c}_{\mathrm{D}}\cdot\boldsymbol{\nabla}\right)\Phi$$

$$-\frac{Ze}{\Omega_c}\frac{\partial F}{\partial E'}(\boldsymbol{\nabla}\Phi\times\hat{\mathbf{n}})\cdot\left(\boldsymbol{\nabla}\mathbf{V}\cdot(c_{\|}\hat{\mathbf{n}}+\mathbf{V}) + (c_{\|}\hat{\mathbf{n}}+\mathbf{V})\cdot\boldsymbol{\nabla}\mathbf{V}\right)$$

$$+\frac{Ze}{M\Omega_c}(\boldsymbol{\nabla}\Phi\times\hat{\mathbf{n}})\cdot\boldsymbol{\nabla}F. \tag{29}$$

Assuming that

$$\Phi(\mathbf{x},t) = \sum_{m=-\infty}^{\infty}\Phi_m(r)\exp[il\zeta - im\theta - i\omega t] \tag{30}$$

and using

$$\begin{bmatrix}\tilde{\Phi}\\ \tilde{f}\end{bmatrix} \equiv \begin{bmatrix}\Phi\\ f\end{bmatrix}\exp[-i(l\zeta-\omega t)] \tag{31}$$

we get

$$\tilde{f} = -\frac{Ze\tilde{\Phi}}{T}F_M + \frac{Ze}{T}F_M\sum_{m=-\infty}^{\infty}e^{-im\theta}\int_{-\infty}^{t}\mathrm{d}t'(il\Omega - i\omega + i\omega_{*T}^{(m)})\Phi_m(r')\times$$

$$\exp\{i[l(\zeta'-\zeta) - m(\theta'-\theta) - \omega(t'-t)]\} \tag{32}$$

Here ζ', θ', r' are evaluated at t', and

$$\omega_{*T}^{(m)} \equiv \omega_*^{(m)} \left[1 + \eta \left(\frac{E'}{T} - \frac{3}{2} \right) + 2\vartheta \frac{\Omega R(c_\parallel + \Omega R)}{2T/M} \right],$$

$$\omega_*^{(m)} \equiv -\frac{m}{r} \frac{cT}{ZeB} \frac{\partial \ln n}{\partial r},$$

$$\eta \equiv \frac{\partial \ln T}{\partial r} \Big/ \frac{\partial \ln n}{\partial r},$$

$$\vartheta \equiv \frac{\partial \ln \Omega}{\partial r} \Big/ \frac{\partial \ln n}{\partial r},$$

$$\text{and } \frac{\mathrm{d}}{\mathrm{d}t} \equiv \frac{\partial}{\partial t} + c_\parallel \hat{\mathbf{n}} \cdot \boldsymbol{\nabla} + \mathbf{V} \cdot \boldsymbol{\nabla} + \mathbf{c}_D \cdot \boldsymbol{\nabla}. \tag{33}$$

However, this form of $\omega_{*T}^{(m)}$ will be insufficient when we consider the E', μ integration. Thus it is appropriate to define:

$$\omega_{*T}^{(m)} = \bar{\omega}_{*T}^{(m)} + \tilde{\omega}_{*T}^{(m)} \frac{c_\parallel}{v_{th}}, \tag{34}$$

where

$$\bar{\omega}_{*T}^{(m)} = \omega_*^{(m)} \left[1 + \eta \left(\frac{E'}{T} - \frac{3}{2} \right) + 2\vartheta \frac{\Omega^2 R^2}{v_{th}^2} \right], \tag{35}$$

$$\text{and } \tilde{\omega}_{*T}^{(m)} = \omega_*^{(m)} \left[2\vartheta \frac{\Omega R}{v_{th}} \right]. \tag{36}$$

III. The Eigenmode Equation

The eigenmode equation is obtained by integrating the drift kinetic equation along unperturbed particle orbits to obtain an expression for the perturbed distribution function. Upon calculating the perturbed density for each species, the quasineutrality condition is used to close the equations and obtain an eigenmode equation.

III.A Integration Along Unperturbed Orbits

In Eq. (32) one can perform the time integration when one knows the expressions $r(t)$, $\theta(t)$, and $\zeta(t)$ along the particle orbit. However, a major difficulty arises due to the fact that the poloidal harmonics, $\Phi_m(r)$, appear inside the integral. Since their form is unknown, the integration is not straightforward.

III.A.1 Long Wavelength Limit

In the limit where the electrostatic perturbations have longer radial scale lengths than particle excursions from the flux surface, we can Taylor expand the poloidal harmonics up to second order in $(r'-r)$, where r and r' denote the radial coordinate of the particle at times t and t'; respectively. This procedure yields:

$$\Phi_m(r') \simeq \Phi_m(r) + (r'-r)\frac{\partial \Phi_m(r)}{\partial r} + \frac{1}{2}(r'-r)^2\frac{\partial^2 \Phi_m(r)}{\partial r^2} + \mathcal{O}(k_r^3\rho_{bi}^3). \qquad (37)$$

Hence, the eigenmode equation describing the time evolution of the perturbed distribution function can be written as:

$$\begin{aligned}\tilde{f} = -\frac{Ze\tilde{\Phi}}{T}F_M + \frac{Ze}{T}F_M \sum_{m=-\infty}^{\infty} e^{-im\theta}\int_{-\infty}^{t} \mathrm{d}t'(il\Omega - i\omega + i\omega_{*T}^{(m)}) \times \\ \exp\{i[l(\zeta'-\zeta) - m(\theta'-\theta) - \omega(t'-t)]\} \times \\ \left[\Phi_m(r) + (r'-r)\Phi_m'(r) + \frac{1}{2}(r'-r)^2\Phi_m''(r)\right] \qquad (38)\end{aligned}$$

where $'$ in Φ_m' corresponds to a radial derivative. We are now able to take $\Phi_m(r)$ outside the integral and the calculation[6,7] of the time dependency of the rest of the quantities is straightforward though tedious.

III.A.2 Particle Drifts

The guiding center drift velocity of particles is given by

$$\mathbf{c}_D = \frac{\hat{\mathbf{n}}}{\Omega_c} \times \left[\frac{Ze}{M} \nabla \Phi_0 + \frac{c_\perp^2}{2} \nabla \ln B + \left(c_\parallel \hat{\mathbf{n}} + \mathbf{V} \right) \cdot \left(\nabla \mathbf{V} + c_\parallel \nabla \hat{\mathbf{n}} \right) \right]. \tag{39}$$

Noting that $\hat{\mathbf{n}} \cdot \nabla \mathbf{V} = \mathbf{V} \cdot \nabla \hat{\mathbf{n}}$, we can write Eq. (39) as:

$$\mathbf{c}_D = \frac{\hat{\mathbf{n}}}{\Omega_c} \times \Big[\underbrace{\frac{Ze}{M} \nabla \Phi_0}_{\mathbf{E}\times\mathbf{B}} + \underbrace{\frac{c_\perp^2}{2} \nabla \ln B}_{\nabla B} + \underbrace{c_\parallel^2 \hat{\mathbf{n}} \cdot \nabla \hat{\mathbf{n}}}_{\text{curvature}} + \underbrace{\mathbf{V} \cdot \nabla \mathbf{V}}_{\text{centrifugal}} + \underbrace{2 c_\parallel \hat{\mathbf{n}} \cdot \nabla \mathbf{V}}_{\text{coriolis}} \Big]. \tag{40}$$

Here Φ_0 is the potential necessary to obtain charge neutrality due to the different centrifugal forces experienced by the ions and electrons. It was defined in Sec. II.A as:

$$Ze\Phi_0 = \alpha \frac{M\Omega^2 R^2}{2}, \tag{41}$$

where $\alpha = \alpha(r)$ is different for each species. The terms in $\mathbf{c}_D$ are given by:

$$\mathbf{V} \cdot \nabla \mathbf{V} = -\Omega^2 R \left(\hat{\mathbf{r}} \cos\theta - \hat{\boldsymbol{\theta}} \sin\theta \right),$$

$$\hat{\mathbf{n}} \cdot \nabla \mathbf{V} = -\Omega (\hat{\mathbf{r}} \cos\theta - \hat{\boldsymbol{\theta}} \sin\theta) - \frac{\epsilon}{q} \Omega \cos\theta \hat{\boldsymbol{\zeta}},$$

$$\frac{Ze}{M} \nabla \Phi_0 = -\alpha \Omega^2 R \left[\frac{\hat{\alpha}}{2} + \hat{\Omega} - \cos\theta \right] \hat{\mathbf{r}} - \alpha \Omega^2 R \sin\theta \hat{\boldsymbol{\theta}},$$

$$\frac{c_\perp^2}{2} \nabla \ln B + c_\parallel^2 \hat{\mathbf{n}} \cdot \nabla \hat{\mathbf{n}} = \frac{1}{R} \left(\frac{c_\perp^2}{2} + c_\parallel^2 \right) \left[-\cos\theta \hat{\mathbf{r}} + \sin\theta \hat{\boldsymbol{\theta}} \right],$$

$$\nabla \mathbf{V} \cdot \hat{\mathbf{n}} = \Omega (\hat{\mathbf{r}} \cos\theta - \hat{\boldsymbol{\theta}} \sin\theta) + \frac{\epsilon}{q} \Omega \cos\theta \hat{\boldsymbol{\zeta}} + \Omega' R \hat{\mathbf{r}},$$

$$\text{and} \quad \nabla \mathbf{V} \cdot \mathbf{V} = \Omega^2 R (\hat{\mathbf{r}} \cos\theta - \hat{\boldsymbol{\theta}} \sin\theta) + \Omega \Omega' R^2 \hat{\mathbf{r}}, \tag{42}$$

where $\hat{\alpha}$ and $\hat{\Omega}$ are defined as:

$$\hat{\Omega} \equiv -\frac{r}{\Omega}\frac{\partial \Omega}{\partial r},$$

$$\text{and} \quad \hat{\alpha} \equiv -\frac{r}{\alpha}\frac{\partial \alpha}{\partial r}. \tag{43}$$

Note that $\hat{\alpha}$ involves derivatives of ion fraction as well as ion temperature. Using the relations in Eq. (42) we get:

$$c_{Dr} = -\frac{\sin\theta}{R_0\,\Omega_c}\left[(1-\alpha)\Omega^2 R_0^2 + 2c_{\|}\Omega R_0 + \left(\frac{c_{\perp}^2}{2} + c_{\|}^2\right)\right],$$

$$c_{D\theta} = -\frac{\cos\theta}{R_0\,\Omega_c}\left[(1-\alpha)\Omega^2 R_0^2 + 2c_{\|}\Omega R_0 + \left(\frac{c_{\perp}^2}{2} + c_{\|}^2\right)\right.$$

$$\left. + \alpha\Omega^2 R_0^2\left(\hat{\Omega} + \frac{\hat{\alpha}}{2}\right)\right],$$

$$\text{and} \quad c_{D\zeta} = -\frac{\epsilon}{q}c_{D\theta}. \tag{44}$$

III.A.3 Particle Excursion

The expression for the excursion of trapped and circulating particles from the flux surface can be calculated using conservation of toroidal canonical angular momentum. Denoting (r,θ) as the position of the particle, and (r_b,θ_b) as the bounce point of trapped particles (with $c_{\|b} \equiv 0$), the conservation law gives:

$$c_{\|}(r,\theta)MR_0(1+\epsilon\cos\theta) + M\Omega(r)R_0^2(1+2\epsilon\cos\theta) - \frac{ZeA_{\zeta}(r)}{c} =$$

$$M\Omega(r_b)R_0^2(1+2\epsilon\cos\theta_b) - \frac{ZeA_{\zeta}(r_b)}{c}, \tag{45}$$

where A_ζ is the toroidal component of the vector potential and we have used $v_\parallel \simeq (c_\parallel + \Omega R)$. Expressing

$$A_\zeta(r) \simeq (r - r_b)\frac{\partial A_\zeta}{\partial r}|_{r_b}, \quad \text{and} \quad \Omega(r) \simeq (r - r_b)\frac{\partial \Omega}{\partial r}|_{r_b}, \tag{46}$$

leads to:

$$r - r_b = \frac{c_\parallel + 2r\Omega\,(\cos\theta - \cos\theta_b)}{\Omega_\theta - \Omega' R}. \tag{47}$$

There are two new terms to be noted in this expression. The first is the orbit squeezing effect introduced in the denominator. For typical tokamak plasmas the angular rotation velocity will be a decreasing function of r, and Ω' will be negative. This effect will be negligible in the core region where the scale length of the angular rotation frequency is comparable to the minor radius. However, it is appropriate to note that it was shown in earlier studies that the orbit squeezing effect can be important in the edge region of H-mode plasmas.[10] Nonetheless this term is retained for completeness in the present analysis even though it has no significant influence on our results. The other term to be noted is the second term in the numerator which is associated with good and bad orbits. It is interesting to point out that since the symmetry is broken by this term, co- or counter-rotation of the plasma can make a difference in the results.

It is evident from Eq. (47) that since $r - r_b$ is periodic in the bounce time τ_b defined in Appendix A, $r - r_b$ can be expressed as a Fourier series in the bounce frequency $\omega_b \equiv 2\pi/\tau_b$. Specifically,

$$r - r_b = \sum_n r^{(n)} e^{in\omega_b t}, \tag{48}$$

and the coefficients $r^{(n)}$ will be given by:

$$r^{(n)} = \frac{1}{\tau_b}\oint_{\text{orbit}} \mathrm{d}t\,(r - r_b)e^{-in\omega_b t}. \tag{49}$$

Introducing an angle-like time variable $\hat{t}$ (see Fig. 1) defined as:

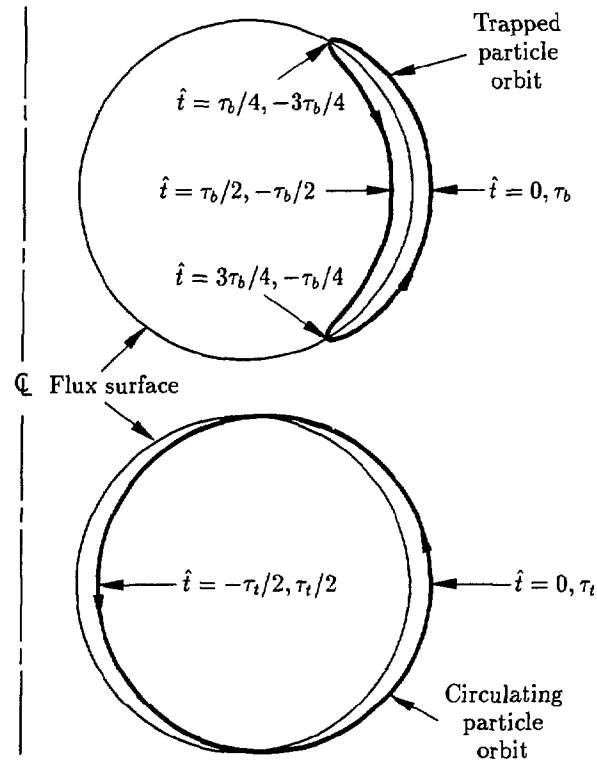

Figure 1: *The angle-like time variable $\hat{t}$ for trapped and circulating particles.*

$$\hat{t}(\theta, \sigma_\parallel = 1) \equiv \frac{R_0 q}{\sqrt{\gamma} v_{th}} \int_0^\theta \frac{d\theta'}{\sqrt{1 - \Lambda/h(\theta)}} \tag{50}$$

$$\hat{t}(\theta, \sigma_\parallel = -1) \equiv \frac{\tau_b}{2} - \hat{t}(\theta, \sigma_\parallel = 1)$$

for trapped particles, and

$$\hat{t}(\theta) \equiv \frac{R_0 q \sigma_{\|}}{\sqrt{\gamma} v_{th}} \int_0^{\theta} \frac{\mathrm{d}\theta'}{\sqrt{1 - \Lambda/h(\theta)}} \tag{51}$$

for circulating particles, we can express $t = t_0 + \hat{t}$, where t_0 is arbitrary. The integral then yields:

$$r^{(n)} = \frac{4 e^{-i n \omega_b t_0}}{\tau_b (\Omega_\theta - \Omega' R_0)} \int_0^{\tau_b/4} \mathrm{d}\hat{t} \left(|c_{\|}| \sin^2 \frac{n\pi}{2} + 2r\Omega \cos\theta \cos^2 \frac{n\pi}{2} \right) \cos n\omega_b \hat{t}, \tag{52}$$

such that

$$r - r_b = \sum_n \hat{r}^{(n)} e^{i n \omega_b \hat{t}}, \tag{53}$$

where

$$\hat{r}^{(n)} = \frac{\sqrt{\epsilon\gamma}}{\pi L_b} \rho'_\theta I_n, \tag{54}$$

$$\rho'_\theta \equiv \frac{v_{th}}{\Omega_\theta - \Omega' R_0}, \quad \text{and} \tag{55}$$

$$I_n = \int_0^{\theta_0} \mathrm{d}\theta \left[\sin^2 \frac{n\pi}{2} + \frac{2\epsilon\varpi}{\sqrt{\gamma}} \frac{\cos\theta}{\sqrt{1 - \Lambda/h(\theta)}} \cos^2 \frac{n\pi}{2} \right] \cos n\omega_b \hat{t}. \tag{56}$$

Here we have introduced the dimensionless variable ϖ defined as:

$$\varpi \equiv \frac{\Omega R_0}{v_{th}}. \tag{57}$$

In Eq. (56) the Jacobian is given by:

$$\frac{\partial\theta}{\partial\hat{t}} = \frac{\sqrt{\gamma} v_{th}}{R_0 q} \sqrt{1 - \Lambda/h(\theta)}, \tag{58}$$

which is a smooth function in the domain of integration. The Fourier series for $r - r_b$ converges as $n \to \infty$ due to the fact that for large values of n, $\cos n\omega_b \hat{t}'$ will be a

rapidly oscillating function. Hence, the integral of this rapidly oscillating term over a smooth function will vanishes as $n \to \infty$; *i.e.*,

$$\lim_{n\to\infty} I_n = 0. \tag{59}$$

III.A.4 Particle Phase

In order to more conveniently perform the integration in time, the particle phase $\exp i[l(\zeta' - \zeta) - m(\theta' - \theta)]$ that appears in Eq. (32) can be expressed as:

$$l(\zeta' - \zeta) - m(\theta' - \theta) = \int_t^{t'} \left(l\frac{\mathrm{d}\zeta}{\mathrm{d}t} - m\frac{\mathrm{d}\theta}{\mathrm{d}t} \right) \mathrm{d}t''. \tag{60}$$

Defining

$$\omega_D \equiv l\frac{\mathrm{d}\zeta}{\mathrm{d}t} - lq\frac{\mathrm{d}\theta}{\mathrm{d}t}, \tag{61}$$

we can approximate this integral as

$$l(\zeta' - \zeta) - m(\theta' - \theta) \simeq \langle \omega_D \rangle_{b/t} (t' - t) + S^{(m)}(\theta' - \theta) - HS^{(m)}\sigma_{\|}\omega_t(t' - t), \tag{62}$$

where

$$S^{(m)}(r) \equiv lq(r) - m \tag{63}$$

with $H = 1$ for circulating particles and $H = 0$ for trapped particles. Using the expressions derived in Sec. III.A.? for $c_{D\theta}$ and $c_{D\zeta}$ it is straightforward to obtain for ω_D:

$$\omega_D \simeq l\Omega - \frac{ql}{r}c_{D_\theta} + \hat{s}\frac{qlc_{\|}}{rR}(r - r_{b/t}), \tag{64}$$

where $\hat{s} \equiv rq'/q$. The calculation of $\langle \omega_D \rangle_{b/t}$ can be performed using the formalism described in Appendix A.

For trapped particles:

$$\langle \omega_D \rangle_b = l\Omega(r_b) + \langle \frac{ql}{r}c_{D\theta} \rangle_b + \langle \frac{ql\hat{s}}{rR_0}c_{\|}(r - r_b) \rangle_b. \tag{65}$$

Using

$$\frac{c_\perp^2}{2} + \frac{c_\parallel^2}{2} = \frac{v_{th}^2}{2}\left[\bar{E} + \frac{\epsilon\bar{g}\cos\theta}{h(\theta)}\right], \tag{66}$$

we get

$$\langle\omega_D\rangle_b = l\Omega(r_b) + \frac{ql}{rR_0\Omega_c}\left\{\langle\cos\theta\rangle_b\left[(1-\alpha)\Omega^2R_0^2 + \frac{v_{th}^2}{2}\bar{E} + \alpha\Omega^2R_0^2(\hat{\Omega}+\frac{\hat{\alpha}}{2})\right]\right.$$

$$\left. + \langle\cos^2\theta\rangle_b\frac{v_{th}^2}{2}\epsilon\bar{g} + \frac{1}{2}\langle c_\parallel^2\cos\theta\rangle_b\right\} + \frac{ql\hat{s}}{rR_0(\Omega_\theta - \Omega' R_0)}\langle c_\parallel^2\rangle_b. \tag{67}$$

Using the expressions derived in Appendix A.0.1 this can be expressed as:

$$\langle\omega_D\rangle_b = l\Omega(r_b) + \frac{lv_{th}^2}{R_0^2\Omega_\theta}\left\{\left(2\frac{E(\kappa)}{K(\kappa)} - 1\right)\left[(1-\alpha)\varpi^2 + \frac{1}{2}\bar{E} + \alpha\varpi^2(\frac{\hat{\alpha}}{2}+\hat{\Omega})\right]\right.$$

$$+ \frac{\epsilon\bar{g}}{2}\left(2\kappa^2\frac{I(\kappa)}{K(\kappa)} - 2\kappa^2\frac{E(\kappa)}{K(\kappa)} + 1\right)$$

$$\left. + \frac{(2\epsilon\gamma)}{2}\left(\kappa^2\frac{I(\kappa)}{K(\kappa)} + (2\kappa^2-1)\frac{E(\kappa)}{K(\kappa)} + 1 - \kappa^2\right)\right\}$$

$$+ \frac{2l\hat{s}\gamma v_{th}^2}{R_0^2(\Omega_\theta - \Omega' R_0)}\left(\frac{E(\kappa)}{K(\kappa)} + \kappa^2 - 1\right). \tag{68}$$

For transit particles we have

$$\langle\omega_D\rangle_t = l\Omega(r_t) + \frac{ql}{rR_0\Omega_c}\left\{\langle\cos\theta\rangle_t\left[(1-\alpha)\Omega^2R_0^2 + \frac{v_{th}^2}{2}\bar{E} + \alpha\Omega^2R_0^2(\hat{\Omega}+\frac{\hat{\alpha}}{2})\right]\right.$$

$$\left. + \langle\cos^2\theta\rangle_t\frac{v_{th}^2}{2}\epsilon\bar{g} + \frac{1}{2}\langle c_\parallel^2\cos\theta\rangle_t\right\}$$

$$+ \frac{ql\hat{s}}{rR_0(\Omega_\theta - \Omega' R_0)}\left[\langle c_\parallel^2\rangle_t - \langle c_\parallel\rangle_t^2 - 2r\Omega\langle c_\parallel\rangle_t\langle\cos\theta\rangle_t\right]. \tag{69}$$

Again, using the expressions derived in Appendix A.0.2 we get:

$$\langle\omega_D\rangle_t = \frac{l v_{th}^2}{R_0^2\,\Omega_\theta}\Bigg\{\left(2\kappa^2\frac{E(\kappa^{-1})}{K(\kappa^{-1})}+1-2\kappa^2\right)\left[(1-\alpha)\varpi^2+\frac{1}{2}\bar{E}+\alpha\varpi^2(\frac{\hat{\alpha}}{2}+\hat{\Omega})\right]$$

$$+\frac{\epsilon\bar{g}}{2}\left(2\kappa^2\frac{I(\kappa^{-1})}{K(\kappa^{-1})}+2\kappa^2(1-2\kappa^2)\frac{E(\kappa^{-1})}{K(\kappa^{-1})}+(1-2\kappa^2)\right)$$

$$+\frac{(2\epsilon\gamma)}{2}\kappa^2\frac{I(\kappa^{-1})}{K(\kappa^{-1})}\Bigg\}+\frac{2l\gamma v_{th}^2\hat{s}}{R_0^2(\Omega_\theta-\Omega' R_0)}\left[\kappa^2\frac{E(\kappa^{-1})}{K(\kappa^{-1})}-\frac{\pi^2\kappa^2}{4K^2(\kappa^{-1})}\right.$$

$$\left.-\sigma_\parallel\frac{\varpi}{\gamma}(2\epsilon\gamma)^{1/2}\frac{\pi\kappa}{2K(\kappa^{-1})}\left(2\kappa^2\frac{E(\kappa^{-1})}{K(\kappa^{-1})}+1-2\kappa^2\right)\right]+l\Omega(r_t) \tag{70}$$

The term $\exp i[S^{(m)}(\theta'-\theta)-HS^{(m)}\sigma_\parallel\omega_t(t'-t)]$ is a periodic function in time with the bounce/transit frequency. Hence it can be written as a Fourier series in the bounce/transit frequency. using the angle-like time variable $\hat{t}$. For trapped particles we can write

$$e^{iS^{(m)}\theta'}=\sum_n \hat{a}^{(n)}e^{in\omega_b\hat{t}'}, \tag{71}$$

and the coefficients are given by:

$$\hat{a}^{(n)}=\frac{1}{\tau_b}\oint_{\text{orbit}}\mathrm{d}\hat{t}'\,e^{iS^{(m)}\theta'-in\omega_b\hat{t}'}. \tag{72}$$

Using the transformation properties of $\hat{t}$ we then get:

$$\hat{a}^{(n)}=\frac{1}{\tau_b}\int_{-\tau_b/4}^{\tau_b/4}\mathrm{d}\hat{t}'\left[(\cos S^{(m)}\theta'+i\sin S^{(m)}\theta')(\cos n\omega_b\hat{t}'-i\sin n\omega_b\hat{t}')\right. \tag{73}$$

$$\left.-(\cos n\pi-i\sin n\pi)(\cos S^{(m)}\theta'+i\sin S^{(m)}\theta')(\cos n\omega_b\hat{t}'+i\sin n\omega_b\hat{t}')\right].$$

The cross terms will yield zero and we can replace $1-\cos n\pi=2\sin^2(n\pi/2)$ and $1+\cos n\pi=2\cos^2(n\pi/2)$ to obtain:

$$\hat{a}^{(n)}=\frac{4}{\tau_b}\int_0^{\tau_b/4}\mathrm{d}\hat{t}'\left[\cos^2\frac{n\pi}{2}\cos S^{(m)}\theta'\cos n\omega_b\hat{t}'+\sin^2\frac{n\pi}{2}\sin S^{(m)}\theta'\sin n\omega_b\hat{t}'\right]. \tag{74}$$

We then get

$$e^{iS^{(m)}(\theta'-\theta)} = \sum_n \hat{a}^{(n)} e^{-iS^{(m)}\theta + in\omega_b \hat{t}'} = \sum_n \hat{a}^{(n)} e^{-i[S^{(m)}\theta - n\omega_b \hat{t}]} e^{in\omega_b(t'-t)} \tag{75}$$

where we have used $\hat{t}' - \hat{t} = t' - t$. We next define a_n such that

$$e^{iS^{(m)}(\theta'-\theta)} = \sum_n a_n e^{in\omega_b(t'-t)} \tag{76}$$

with

$$a_n = e^{-i[S^{(m)}\theta - n\omega_b \hat{t}]} \frac{\sqrt{\epsilon}}{\pi L_b} J_{n,m} \tag{77}$$

and

$$J_{n,m} = \int_0^{\theta_0(\Lambda)} \frac{\mathrm{d}\theta'}{\sqrt{1-\Lambda/h(\theta)}} \left[\cos^2\frac{n\pi}{2} \cos S^{(m)}\theta' \cos n\omega_b \hat{t}' + \sin^2\frac{n\pi}{2} \sin S^{(m)}\theta' \sin n\omega_b \hat{t}'\right]. \tag{78}$$

Proceeding with a similar analysis for circulating particles, we have:

$$e^{i[S^{(m)}\theta' - \sigma_\parallel S^{(m)}\omega_t \hat{t}']} = \sum_n \hat{a}^{(n)} e^{in\omega_t \hat{t}'}, \tag{79}$$

and the coefficients $\hat{a}^{(n)}$ are given by:

$$\hat{a}^{(n)} = \frac{1}{\tau_t} \int_{-\tau_t/2}^{\tau_t/2} \mathrm{d}\hat{t}' \left(\cos[S^{(m)}\theta' - (n+\sigma_\parallel S^{(m)})\omega_t \hat{t}'] + i \sin[S^{(m)}\theta' - (n+\sigma_\parallel S^{(m)})\omega_t \hat{t}']\right). \tag{80}$$

However, the sin[...] integral will vanish and we are left with

$$\hat{a}^{(n)} = \frac{2}{\tau_t} \int_0^{\tau_t/2} \mathrm{d}\hat{t}' \cos[S^{(m)}\theta' - (n+\sigma_\parallel S^{(m)})\omega_t \hat{t}'], \tag{81}$$

such that the phase can be expressed as

$$e^{i[S^{(m)}(\theta'-\theta) - \sigma_\parallel S^{(m)}\omega_t(t'-t)]} = \sum_n a_n e^{in\omega_t(t'-t)}. \tag{82}$$

Defining

$$K_{n,p,m} = \int_0^\pi \frac{\mathrm{d}\theta'}{\sqrt{1-\Lambda/h(\theta)}} \cos\left[S^{(p)}\theta' - (n+\sigma_\parallel S^{(m)})\omega_t\hat{t}'\right], \tag{83}$$

a_n is given by:

$$a_n = \frac{\sqrt{\epsilon}}{\pi L_t} e^{-i[S^{(m)}\theta - (n+\sigma_\parallel S^{(m)})\omega_t\hat{t}]} K_{n,m,m}. \tag{84}$$

III.A.5 Time Integration

Having formulated the particle phase and radial excursion as a Fourier series, we can now perform the time integration, keeping in mind that the perturbation vanishes at $t = -\infty$. Hence, the perturbed distribution function becomes:

$$\tilde{f} = -\frac{e\tilde{\Phi}}{T}F_M + \frac{eF_M}{T}\sum_m e^{-im\theta}(\omega - l\Omega - \omega_{*T}) \times \tag{85}$$

$$\sum_n a_n \left\{ \Phi_m G(n) + \Phi'_m \sum_{n_1} \hat{r}_{n_1} e^{in_1\omega_b\hat{t}} \left[G(n+n_1) - G(n)\right] \right.$$

$$\left. + \frac{1}{2}\Phi''_m \sum_{n_1,n_2} \hat{r}_{n_1}\hat{r}_{n_2} e^{i(n_1+n_2)\omega_b\hat{t}} \left[G(n+n_1+n_2) - 2G(n+n_1) + G(n)\right] \right\},$$

where $G(n)$ is defined as:

$$G(n) \equiv \frac{1}{\omega - (\omega_D)_{b/t} - (n + H\sigma_\parallel S^{(m)})\omega_{b/t} + i\nu}. \tag{86}$$

III.B Quasineutrality Condition

The perturbed distribution function for each species is integrated over velocity space to produce the perturbed densities. The quasineutrality condition is then simply

$$\tilde{n}_e = \sum_{j\neq e} Z_j \tilde{n}_j, \tag{87}$$

which can be cast in the form

$$\sum_m e^{-im\theta}\left[P_m(r,\theta)\Phi_m''(r) + Q_m(r,\theta)\Phi_m'(r) + R_m(r,\theta)\Phi_m(r)\right] = 0. \tag{88}$$

In order to eliminate the explicit θ-dependence in this equation, a Fourier transform is performed to obtain a set of coupled ordinary differential equations involving $\Phi_m(r)$. This is carried out by operating with $(2\pi)^{-1}\int_{-\pi}^{\pi} d\theta\, e^{ip\theta}$ on the quasineutrality equation thereby generating equations of the form:

$$\sum_m A_{pm}\Phi_m''(r) + B_{pm}\Phi_m'(r) + C_{pm}\Phi_m(r) = 0. \tag{89}$$

In the evaluation of the coefficients we consider the radial excursions of the trapped ions to be dominant, with those of circulating ions being smaller by a factor of $\mathcal{O}(\epsilon^{1/2})$ and those of electrons being smaller by a factor of $\mathcal{O}(\sqrt{M_e/M_i})$. In other words, the coefficients A_{pm} and B_{pm} will only involve contribution from trapped ions. For the coefficient C_{pm} which also includes the adiabatic response through the first term in Eq. (85), we assume that the non-adiabatic circulating electron response is negligible. Due to the fact that electrostatic and centrifugal trapping occur with sheared rotation, the velocity space integration must be carried out with special care. The integration limits and the order of the velocity integration combined with the Fourier transform is discussed in Appendix B. The choice for the integration order is dictated by the most suitable form for the numerical calculation of the integrals.

III.B.1 Adiabatic Density Response

The adiabatic part of the perturbed distribution function in Eq. (85) is

$$\tilde{f}^{\text{adiab.}} = -e\tilde{\Phi}F_M/T. \tag{90}$$

Integration over velocity space will then yield:

$$\tilde{n}^{\text{adiab.}} = \int 2\pi c_\perp dc_\perp dc_\parallel \left[-\frac{Ze\tilde{\Phi}F_M}{T}\right] = -n_0 \exp(\epsilon\bar{g}\cos\theta)\frac{e\tilde{\Phi}}{T}, \tag{91}$$

where n_0 was defined in Sec. II.A. Using the expansion for $\tilde{\Phi}$, the Fourier transform is given by:

$$\tilde{n}_{p,m}^{\text{adiab.}} = \frac{1}{2\pi}\int_{-\pi}^{\pi} \mathrm{d}\theta\, n_0\, \exp[\epsilon\bar{g}\cos\theta]\, \exp[i(p-m)\theta]\, \frac{e\Phi_m}{T}. \tag{92}$$

We can expand the exponential to $\mathcal{O}(\epsilon\bar{g})$ and get:

$$\tilde{n}_{p,m}^{\text{adiab.}} = n_0 \frac{e\Phi_m}{T}\left[\delta_{p,m} + \frac{\epsilon\bar{g}}{2}(\delta_{p,m-1} + \delta_{p,m+1})\right]. \tag{93}$$

After appropriate normalization with respect to T_e, n_{0e}, and e, the contribution of the adiabatic density response to $C_{p,m}$ is given by a sum over all species:

$$C_{p,m}^{\text{adiab.}} = \sum_j Z_j^2 f_j \tau_j \left[\delta_{p,m} + \frac{\epsilon\bar{g}}{2}(\delta_{p,m-1} + \delta_{p,m+1})\right] \tag{94}$$

where the j summation includes electrons.

III.B.2 Non-Adiabatic Density Response

As noted earlier, we consider only the contribution from trapped ions in the calculation of $A_{p,m}$. In the expression for $\omega_{*T}^{(m)}$ (see Eq. (34)), the parallel velocity dependent part, *i.e.*, $\tilde{\omega}_{*T}^{(m)} c_\parallel / v_{th}$, is cancelled by $\sum_{\sigma_\parallel}$, thereby leading to:

$$\begin{aligned} A_{p,m} = \sum_j^{\text{ions}} Z_j^2 f_j \tau_j \int_{1-\epsilon}^{1+\epsilon} \mathrm{d}\Lambda \int_0^\infty \mathrm{d}Y \frac{(Y + \bar{g}_j/\Lambda)^{3/2}\epsilon^{3/2}{\rho'_{\theta j}}^2}{2\pi^{9/2}L_b^3} \exp\left[-Y + \bar{g}_j\frac{\Lambda-1}{\Lambda}\right] \times \\ \times \sum_n \frac{(\omega - l\Omega - \tilde{\omega}_{*T}^{(m)})}{\omega - \langle\omega_{Dj}\rangle_b - n\omega_{bj} + i\nu_j} \times \\ \times \sum_{n_1,n_2} I_{n_1} I_{n_2} \left[J_{n-n_1-n_2,m} J_{n,p} - 2J_{n-n_1,m} J_{n+n_2,p} + J_{n,m} J_{n+n_1+n_2,p}\right]. \end{aligned} \tag{95}$$

Similar to the calculation of $A_{p,m}$, the only contribution to $B_{p,m}$ comes from trapped ions:

$$B_{p,m} = \sum_j^{\text{ions}} Z_j^2 f_j \tau_j \int_{1-\epsilon}^{1+\epsilon} d\Lambda \int_0^\infty dY \frac{\epsilon \rho'_{\theta j}(Y + \bar{g}_j/\Lambda)}{\pi^{7/2} L_b^2} \exp\left[-Y + \bar{g}_j \frac{\Lambda - 1}{\Lambda}\right] \times$$

$$\sum_n \frac{(\omega - l\Omega - \bar{\omega}_{*T}^{(m)})}{\omega - \langle \omega_{Dj} \rangle_b - n\omega_{bj} + i\nu_j} \sum_{n_1} I_{n_1} \left[J_{n,p} J_{n-n_1,m} - J_{n+n_1,p} J_{n,m}\right]. \quad (96)$$

The non-adiabatic portion of $C_{p,m}$ can be written as

$$C_{p,m}^{\text{non-adb.}} = C_{p,m}^{\text{trapped}} + C_{p,m}^{circ-1} + C_{p,m}^{circ-2}. \quad (97)$$

with the first term being the trapped particle response, the second term corresponding to the integral involving $\bar{\omega}_{*T}^{(m)}$ as defined in Eq. (35), and the third term corresponding to the integral involving $\tilde{\omega}_{*T}^{(m)}$ defined in Eq. (36). For the trapped particle term we obtain:

$$C_{p,m}^{\text{trapped}} = \sum_j Z_j^2 f_j \tau_j \int_{1-\epsilon}^{1+\epsilon} d\Lambda \int_0^\infty dY \frac{\epsilon^{1/2}(Y + \bar{g}_j/\Lambda)^{1/2}}{\pi^{5/2} L_b} \exp\left[-Y + \bar{g}_j \frac{\Lambda - 1}{\Lambda}\right] \times$$

$$\times \sum_n \frac{(\omega - l\Omega - \bar{\omega}_{*T}^{(m)})}{\omega - \langle \omega_{Dj} \rangle_b - n\omega_{bj} + i\nu_j} J_{n,p} J_{n,m}. \quad (98)$$

Similarly, the parallel velocity independent circulating particle term is straightforwardly calculated; *i.e.*,

$$C_{p,m}^{\text{circ}-1} = \sum_j Z_j^2 f_j \tau_j \int_0^{1-\epsilon} d\Lambda \int_0^\infty dY \frac{\epsilon^{1/2}(Y + \bar{g}_j/\Lambda)^{1/2}}{\pi^{5/2} L_t} \exp\left[-Y + \bar{g}_j \frac{\Lambda - 1}{\Lambda}\right] \times$$

$$\times \sum_n \frac{(\omega - l\Omega - \bar{\omega}_{*T}^{(m)})(\omega + i\nu_j)}{(\omega + i\nu_j)^2 - [(n + S^{(m)})\omega_t]^2} K_{n,p,m} K_{n,m,m}. \quad (99)$$

However, for the parallel velocity dependent part of the circulating response we encounter a θ integral which cannot be expressed in terms of the Fourier coefficients

introduced in Sections III.A.3 and III.A.4. To deal with this problem it is convenient to define:

$$M_{n,p,m} \equiv \int_0^{\pi} \cos\left[S^{(p)}\theta - (n + S^{(m)})\,\omega_t \hat{t}(\theta)\right] \mathrm{d}\theta. \tag{100}$$

This leads readily to the result:

$$C_{p,m}^{\mathrm{circ}-2} = \sum_j Z_j^2 f_j \tau_j \int_0^{1-\epsilon} \mathrm{d}\Lambda \int_0^{\infty} \mathrm{d}Y \frac{\epsilon^{1/2}(Y + \bar{g}_j/\Lambda)}{\pi^{5/2} L_t} \exp\left[-Y + \bar{g}_j \frac{\Lambda - 1}{\Lambda}\right] \times$$

$$\times \sum_n \frac{[(n + S^{(m)})\omega_t](-\tilde{\omega}_{*T}^{(m)})}{(\omega + i\nu_j)^2 - [(n + S^{(m)})\omega_t]^2} M_{n,p,m} K_{n,m,m}. \tag{101}$$

Hence, $C_{p,m}$ is given by:

$$C_{p,m} = C_{p,m}^{\mathrm{adiab.}} + C_{p,m}^{\mathrm{trapped}} + C_{p,m}^{\mathrm{circ}-1} + C_{p,m}^{\mathrm{circ}-2}. \tag{102}$$

III.C Boundary Conditions

The two-dimensional eigenmode equation formulated in the preceding sections as a set of coupled second order differential equations requires proper boundary conditions in the domain $r \in [0, a]$. Since the boundary conditions originally chosen by Marchand[6] remain appropriate in the presence of sheared equilibrium flows, we can again select the boundary conditions for each poloidal harmonic to be given by:

$$\Phi_m(a) = 0, \quad \text{for all } m, \tag{103}$$

$$\Phi_m(0) = 0, \quad \text{for } m \neq 0, \tag{104}$$

$$\left.\frac{\partial \Phi_0}{\partial r}\right|_{r=0} = 0, \tag{105}$$

which correspond to a conducting wall at $r = a$ and would cause no charge accumulation on axis, $r = 0$. In practice, though, we allow the more general conditions

$\Phi_m(r_L) = \Phi_m(r_R) = 0$, where $0 \leq r_L < r_R \leq a$, and perform the calcution only in this interval. Having assigned the boundary conditions, the problem is overspecified due to the fact that this is a homogeneous equation; *i.e.*, $\Phi(r, \theta, t) = 0$ is a solution of the equation. Hence, there exists a non-zero solution only for certain values of the mode frequency ω, thereby making this an eigenvalue problem.

III.D Numerical Solution Method

A finite element method with cubic-B splines as finite elements has been used for the numerical solution of this set of coupled differential equations. Since this procedure has already been described in detail in Ref. 6, it is not necessary to repeat it here. An important modification to Marchand's method is the choice of grid spacing. Rather than equally spaced grid points, the grid density is increased near the rational surfaces. This is motivated by the recognition that each poloidal harmonic displays its largest structure near its corresponding rational surface. It is in fact found that the same level of accuracy is achieved with fewer gridpoints when this variable grid spacing is employed.

IV. Numerical Results

IV.A Equilibrium Profiles

For a realistic analysis of shear flow effects on the trapped ion instability we consider representative experimental data from TFTR for the density, temperature, and q-profiles. The data is obtained from a TRANSP run at 3.00 sec. of TFTR (L-mode) shot #49982. Even though our numerical scheme can deal with multiple ion species, we concentrate here on the basic case with a single ion species; *e.g.*, a deuterium plasma. Since accurate velocity profile data was not available, the profile chosen for the toroidal rotation velocity corresponds to the ion temperature profile. This seems to be a reasonable choice, since most experimental measurements indicate

that the ion toroidal momentum diffusion coefficient, χ_ϕ, and the energy transport transport coefficient, χ_i, are very similar in their radial variations. Measurements of $T_i(r)$ and $V_\phi(r)$ profiles in DIII-D plasmas also support this trend.[11] Accordingly, the angular rotation frequency Ω is chosen to be:

$$\Omega(r) = M_0 \frac{v_{thi}(0)}{R_0} \frac{T_i(r)}{T_i(0)}. \tag{106}$$

Here, for $M_0 = 1$, the angular rotation velocity on axis ($r = 0$) would correspond to Mach number 1. Thus, the parameter we vary in this analysis is M_0, which is termed "the Mach number on axis".

The equilibrium profiles for n, T_e, T_i, and q vs. r/a are plotted in Fig. 2. The largest drive for the mode is expected to come from the region around $r/a = 0.55$, where the local value for η_i is $\eta_i \sim 7$. Hence, we expect the mode to be localized in this region.

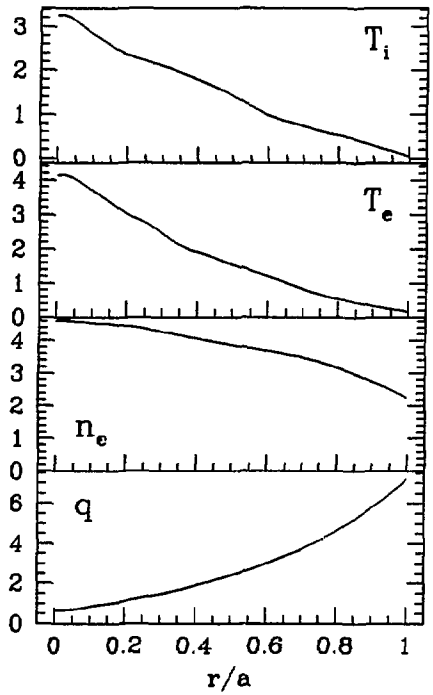

Figure 2: *Equilibrium density, temperature and q-profiles for the TFTR L-mode shot # 49982.*

IV.B Single Poloidal Harmonic Case

To isolate the effects of sheared toroidal flows on the trapped ion instability, we first study the simplest limit where only a single poloidal harmonic is considered. Although our analysis is formulated to deal with the general case of poloidal mode coupling in toroidal geometry, it is possible to chose a q-profile for which the mode rational surfaces are spaced a large distance apart. This would then correspond to a sheared slab geometry analysis with toroidal effects like trapped particles, magnetic drifts etc. artificially included in the model. Here we follow an easier path by artificially turning off the off-diagonal elements of the $A_{p,m}$, $B_{p,m}$, and $C_{p,m}$ matrices. In this way, the equations become decoupled. Due to the nature of the problem, the eigenvalue satisfying the equation for Φ_{m_0}, $\omega^{(m_0)}$, will result in $\Phi_{m\neq m_0} = 0$. This analysis is also useful in identifying the "parent" mode of a fully coupled eigenmode. By decreasing the masking multiplier of the off-diagonal elements from 1 to 0, one will end up with a single poloidal harmonic, which can be called the parent mode.

For TFTR L-mode parameters, the $l = 2$, $m = 5$ single poloidal harmonic case is analyzed. The parameter M_0 corresponding to the Mach number on axis is varied between -0.25 and 0.25. As explained earlier, the angular rotation frequency profile is taken to be the same as the ion temperature profile. It is scaled to give the corresponding value of M_0 as described in the previous section. In Fig. 3 the growth rate, γ, and the real frequency in the moving frame, $\omega_r - l\Omega(r_0)$, are plotted against the rotation parameter M_0. The real frequency of the mode involves a large Doppler shift corresponding to the level of rotation where the mode is maximized, *e.g.*, around $r/a \simeq 0.55$ for the TFTR L-mode parameters. Hence, a plot of ω_r versus the Mach number on axis, M_0, yields an almost straight line, since the Doppler shift in the frequency dominates all other variations associated with shear flow effects. For this purpose, rather than plotting the real frequency itself, the Doppler corrected frequency is plotted. This is obtained by choosing an appropriate radial location r_0 such that $\omega_r - l\Omega(r_0)$ displays the most structure with respect to M_0. This quantity

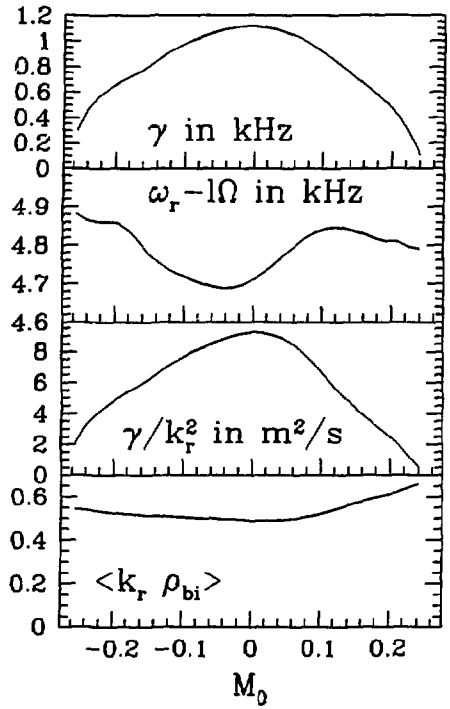

Figure 3: *Growth rate, γ, real frequency in the moving frame, $\omega_r - l\Omega$, transport estimate, γ/k_r^2, and average radial wavenumber, $k_r\rho_{bi}$, vs. the Mach number on axis, M_0, for TFTR L-mode parameters, $l = 2$ and the single poloidal harmonic $m = 5$.*

is termed the "real frequency in the moving frame". As discussed in Sec. III.A.3, a difference between co- and counter rotation is expected. Results here indicate a modest difference of this type along with a significant stabilizing effect with respect to the shear flow parameter M_0.

The values of the average radial wavenumber $\langle k_r\rho_{bi}\rangle$ and the heuristic anomalous

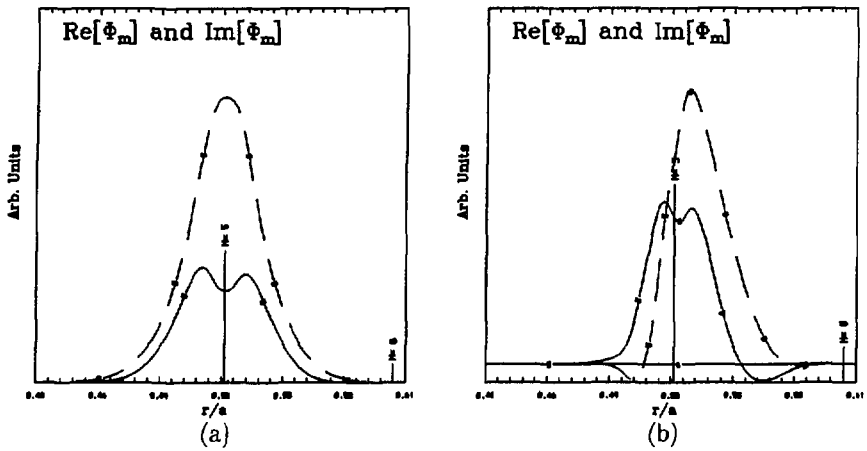

Figure 4: *Eigenfunctions of the single poloidal harmonic case ($l = 2$, and $m = 5$) with TFTR L-mode data. (a) $M_0 = 0$.; (b) $M_0 = 0.24$.*

diffusivity estimate $\langle \gamma / k_r^2 \rangle$ vs. the Mach number on axis, M_0, are plotted in Fig. 3. The decrease in the transport estimate by sheared toroidal rotation is due to both the reduction in the growth rate γ and the increasing radial wavenumber. The mode structures for a case with rotation and one without rotation are shown in Fig. 4. Here, for $M_0 = 0.2$, the mode is narrower compared to the $M_0 = 0$ case. We also observe that for the case with sheared rotation, the mode is localized slightly away from the rational surface corresponding to $l = 2$, $m = 5$.

IV.C Fully Coupled Cases

Using the equilibrium profiles described in Sec. IV.A, the most realistic fully coupled cases for toroidal mode numbers $l = 2$ and $l = 4$ are analyzed. In these cases, the model angular rotation profile which scales as the ion temperature is again used. The primary finding is that the trapped ion instability is significantly stabilized for $M_0 \sim 0.2$, the Mach number on axis. This result is in line with the findings for the ion temperature gradient mode in simple sheared slab geometry studies, as well as with the single poloidal harmonic case described in the previous section. In what follows, the numerical results pertaining to each toroidal mode number are given in detail.

IV.C.1 Toroidal mode number $l = 2$

The $l = 2$ case is one of the simpler cases considered. This is due to the fact that since there are very few rational surfaces in the region of free energy, the associated numerical analysis is much easier to implement. As in the single poloidal harmonic case of Sec. IV.B, the parameter varied is the Mach number on axis, M_0. Keeping three poloidal harmonics $m = 4, \ldots, 6$ with the nonuniform grid scheme, the rotation parameter M_0 is varied between -0.2 and 0.2. In Fig. 5 the growth rate γ is plotted vs. M_0. The stabilizing influence of sheared rotation is evident from this figure.

Specifically, the growth rate is reduced by half for a rotation value of $M_0 \sim 0.15$. The real frequency in the rotating frame $\omega_r - l\Omega(r_0)$ vs. M_0 is also plotted in Fig. 5 along with the average radial wavelength in terms of the ion banana radius and the transport estimate $\langle \gamma / k_r^2 \rangle_r$. Similar to the case in Sec. IV.B the decreasing growth rate is accompanied by an increase in the radial wave-number (or decrease in mode width), such that the transport estimate is reduced even further. The radial structures of the poloidal harmonics at selected rotation values are plotted in Fig. 6. Compared with the $M_0 = 0$ case, the mode widths of the individual poloidal harmonics are significantly reduced for the $M_0 = 0.2$ case.

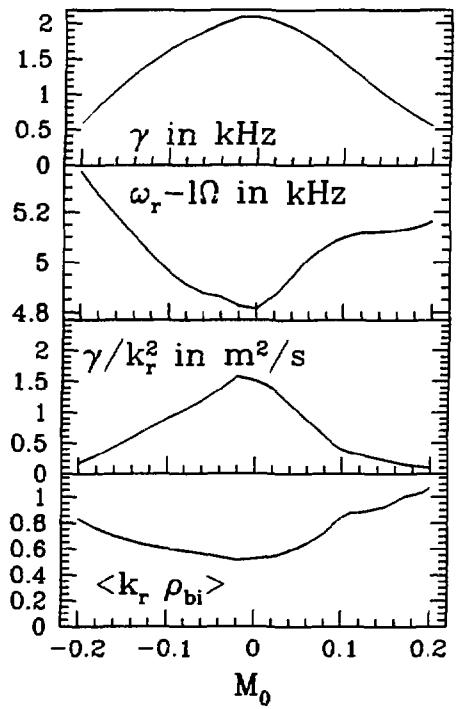

Figure 5: *Growth rate, γ, real frequency in the moving frame, $\omega_r - l\Omega$, transport estimate, γ/k_r^2, and average radial wavenumber, $k_r\rho_{bi}$, vs. the Mach number on axis, M_0, for TFTR L-mode parameters and toroidal mode number $l = 2$.*

An interesting feature of sheared toroidal rotation is shown in Fig. 7. Here, a contour plot of the poloidal cross section of the eigenmode is plotted at the rotation values corresponding to Fig. 6. In the absence of rotation, the eddies in the bad curvature region (the outside of the tokamak, $\theta \in [-\pi/2, \pi/2]$) point outwards and have significant radial extent. However, as the rotation parameter is increased, the

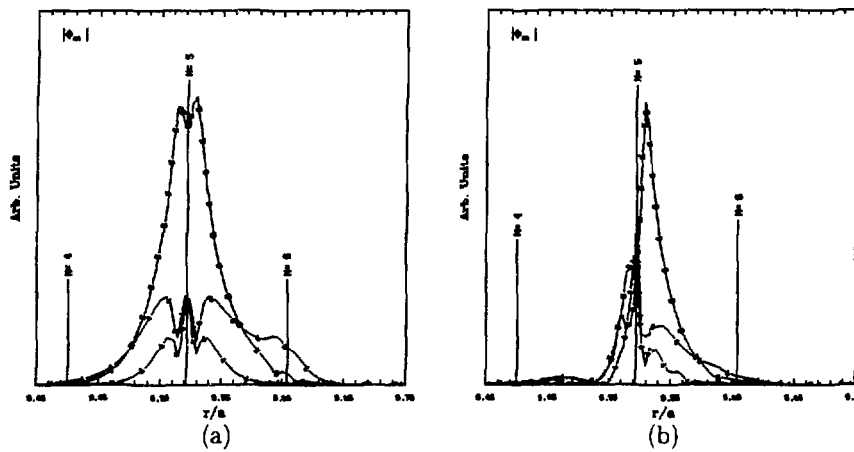

Figure 6: *Eigenfunctions corresponding to Fig. 5. (a)* $M_0 = 0$*; (b)* $M_0 = 0.2$.

eddies in the bad curvature region get twisted and the radial extent is much narrower. A poloidal asymmetry also develops, which of course depends on the sign of the toroidal mode number, l.

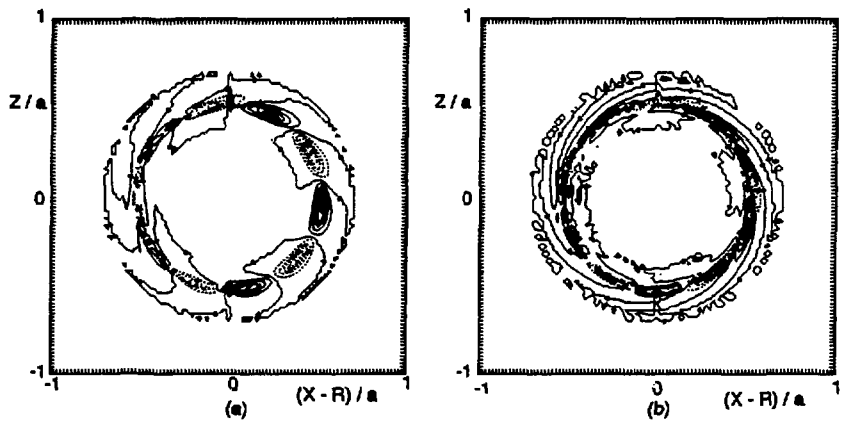

Figure 7: *Poloidal cross-section of the eigenfunctions corresponding to Fig. 5. (a)* $M_0 = 0$*; (b)* $M_0 = 0.2$.

IV.C.2 Toroidal mode number $l = 4$

For the same equilibrium configuration as in the $l = 2$ case of Sec. IV.C.1, sheared toroidal rotation has a significant stabilizing effect on the $l = 4$ case. Using the poloidal harmonics $m = 8, \ldots, 12$, the toroidal rotation parameter M_0 is varied from -0.1 to 0.1. In Fig. 8 the growth rate is plotted against the Mach number on axis, M_0. Much like the $l = 2$ case, the growth rate decreases as toroidal rotation is increased. Slight asymmetry in the growth rate with respect to the direction of toroidal rotation is visible in Fig. 8. This asymmetry is basically due to trapped particle orbit effects, *i.e.*, good and bad particle orbits associated with co- and counter-rotation. The real frequency in the rotating frame for this case is plotted in Fig. 8.

The average radial wavenumber $\langle k_r \rho_{bi} \rangle$, and the transport estimate are also shown in Fig. 8. The highest value for the Mach number that can be analyzed using our code can be obtained by inspection of Fig. 8. For $|M_0| \approx 0.1$, the average wavenumber $\langle k_r \rho_{bi} \rangle \to 1$ where the differential approximation breaks down. Fig. 8 indicates that the transport estimate is more favorably affected by co-rotation ($M_0 > 0$) compared to counter-rotation ($M_0 < 0$).

The corresponding eigenfunctions for the $l = 4$ case are given in Fig. 9 for $M_0 = 0$ and $M_0 = 0.1$. The locations of the rational surfaces corresponding to the poloidal mode numbers $m = 8, \ldots, 12$ are also indicated in this figure. The individual poloidal harmonics are localized around their associated rational surfaces. In Fig. 9 it is evident that the mode gets narrower with increasing toroidal rotation. In the absence of rotation ($M_0 = 0$), the dominant poloidal harmonics are $m = 10$ and $m = 11$. For co-rotation, $M_0 > 0$, the mode is shifted inward (Fig. 9), and the dominant poloidal harmonic is now $m = 10$.

The poloidal cross-sections of the eigenfunctions for the same rotation values as in Fig. 9 are plotted in Fig. 10. For the $l = 4$ case, the structure of the outward pointing eddies in the bad curvature region is more pronounced compared to the eigenfunctions of the $l = 2$ case plotted in Fig. 7. The effect of toroidal rotation on

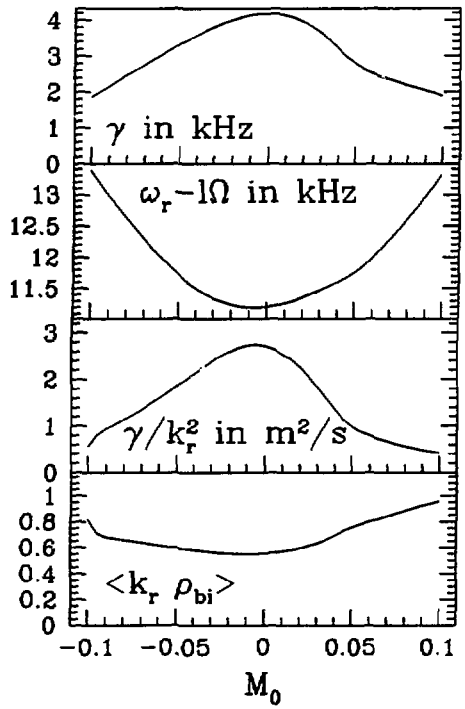

Figure 8: *Growth rate, γ, real frequency in the moving frame, $\omega_r - l\Omega$, transport estimate, γ/k_r^2, and average radial wavenumber, $k_r\rho_{bi}$, vs. the Mach number on axis, M_0, for TFTR L-mode parameters and toroidal mode number $l = 4$.*

the poloidal mode structure is visible in Fig. 10b. The eddies become twisted in the poloidal direction and narrower in the radial direction. Note that the eigenmode is no longer poloidally symmetric.

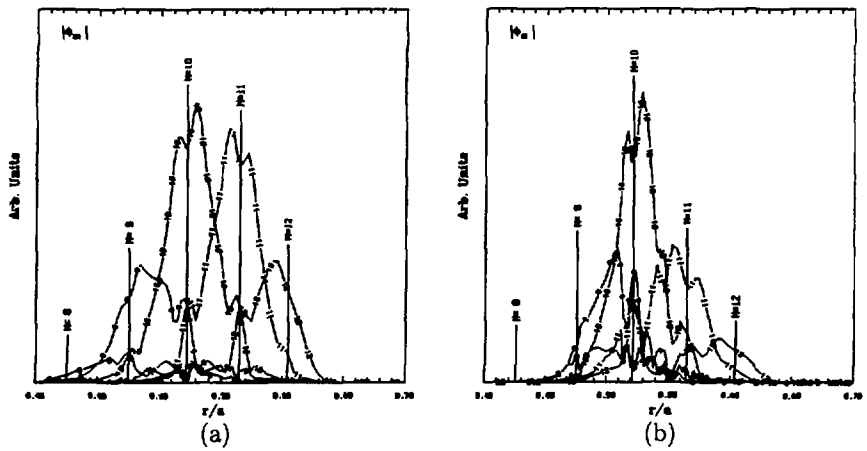

Figure 9: *Poloidal cross-section of the eigenfunctions corresponding to Fig. 8. (a)* $M_0 = 0$*; (b)* $M_0 = 0.1$.

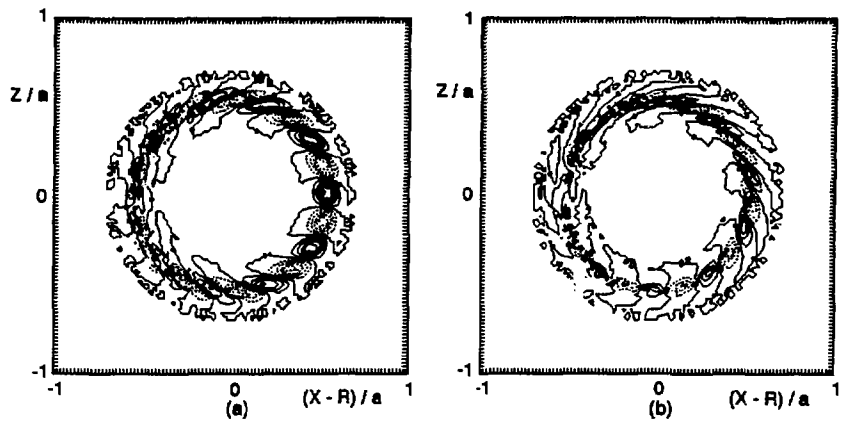

Figure 10: *Poloidal cross-section of the eigenfunctions corresponding to Fig. 5. (a)* $M_0 = 0$*; (b)* $M_0 = 0.1$.

IV.D Beam Species

The effects of toroidal rotation in the presence of a beam species are illustrated in Fig. 11. For this analysis, experimental profiles of electron density and temperature, and beam density and temperature along with main ion temperature are used. The main ion density is calculated by the relation $n_i = n_e - \alpha_b n_b$ where α_b is the beam density multiplier. Three cases are presented corresponding to $\alpha_b = 0, 1, 2$. Hence, this means that for $\alpha_b = 0$ we ignore beam ions, for $\alpha_b = 1$ we use actual experimental data, and for $\alpha_b = 2$, the hypothetical case of double the experimental beam ion density is considered.

It is found that in the absence of toroidal rotation (for $M_0 = 0$) the linear growth rate decreases as the beam ion density is increased. This is the expected dilution effect since the instability is mainly coming from the free energy in the main ion population whose fraction is now reduced. However, when toroidal rotation is present, the presence of beam ions actually reduces the stabilizing influence of sheared flows. This trend can be understood by recalling the fact that the instability drive of the beam ion population, although smaller than that of the main ion population, is not affected by sheared flows, since the average thermal speed of beam ions is significantly larger than the flow velocity.

V. Summary and Discussion

An important area of current research deals with the question of what is the actual spatial extent of the turbulence controlling anomalous transport in tokamaks. The prevalent view has been that anomalous transport is primarily driven by electrostatic microinstabilities whose spatial extent is typically several ion-gyroradii. This leads to a so-called Gyro-Bohm scaling of confinement. However, more recent experimental evidence from TFTR and DIII-D along with theoretical studies of long-wavelength turbulence suggests that Bohm-scaling could be dominant and that the associated

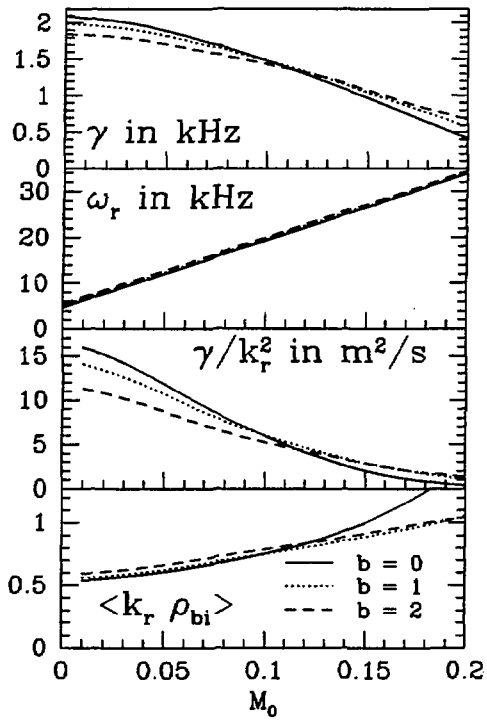

Figure 11: *Growth rate, real frequency, radial wavenumber, and transport estimate vs. toroidal rotation parameter, in the presence of beam ions.*

spatial scale should be on the equilibrium (plasma radial dimension) length scale. In the present paper we have presented the first gyrokinetic toroidal analysis of the influence of sheared toroidal rotation on the electrostatic trapped ion mode. The two-dimensional linear treatment of these important long wavelength instabilities has been performed using a finite element code to calculate the eigenfunction and the eigenfrequency associated with a chosen toroidal mode number. The equilibrium quantities are taken from experimental data, *i.e.*, representative TFTR L-mode profiles were used.

The principal results indicate that both the linear growth rates as well as the radial correlation lengths are decreased in the presence of sheared toroidal rotation. The changes in the heuristic estimates of diffusivity, γ/k_r^2, are even more pronounced since a decrease in the growth rate is associated with an increase in the radial wavenumber. These trends are in reasonable agreement with results from recent BES (beam emission spectroscopy) measurements of long-wavelength turbulence in TFTR plasmas.[12]

It can be concluded that for toroidal rotation velocities comparable to a fraction of the main ion thermal velocity and with velocity shear scales comparable to the ion temperature scale length, the longest wavelength portion of trapped ion instability spectrum can be significantly stabilized. The limitation of the present analysis is that only modes with radial wavelengths longer than the ion banana width can be analyzed. In order to deal with the shorter perpendicular wavelengths, *i.e.*, for larger toroidal mode numbers, an integral eigenmode analysis including FLR effects is necessary. For present day computer capabilities this is a formidable task. Even though the ballooning formalism has been effectively employed for high toroidal mode numbers in the absence of strong toroidal rotation,[13] in the presence of strong toroidal rotation it is not applicable to the shear flow problem in a straightforward manner due to the fact that the large Doppler shift in the real part of the eigenfrequency breaks the ballooning approximation that the mode frequency has only small variations across magnetic surfaces.

Acknowledgments

This work was supported by the United States Department of Energy Contract No. DE-AC02-76-CHO-3073.

Appendix A. Averages over particle orbits

Using the definitions of $c_{\|}$, Λ, and γ given in Sec. II.A we can calculate certain averages over particle orbits. The material presented here is taken from Ref. 6 with shear flow modifications.

A.0.1 Trapped particles

Defining

$$2\kappa^2 = 1 + \frac{1-\Lambda}{\epsilon}, \tag{A1}$$

the parallel velocity can be expressed as:

$$c_{\|} = \sigma_{\|} v_{th} \epsilon^{1/2} \gamma^{1/2} \sqrt{2\kappa^2 - 1 + \cos\theta}. \tag{A2}$$

The bounce frequency is defined as

$$\tau_b \equiv \oint_{\text{orbit}} \frac{\mathrm{d}\theta}{\dot{\theta}}. \tag{A3}$$

Using $\dot{\theta} \simeq c_{\|}/R_0 q$ this can be expressed as:

$$\tau_b = \frac{4R_0 q}{v_{th}(\epsilon\gamma)^{1/2}} \int_0^{\theta_0} \frac{\mathrm{d}\theta}{\sqrt{2\kappa^2 - 1 + \cos\theta}}. \tag{A4}$$

Using the transformation $\sin(\theta/2) = \kappa \sin\xi$ gives

$$\mathrm{d}\theta = \frac{2\kappa \cos\xi \mathrm{d}\xi}{\sqrt{1 - \kappa^2 \sin^2\xi}}. \tag{A5}$$

In terms of ξ we get:

$$c_{\|} = (\epsilon\gamma)^{1/2} v_{th} \sqrt{2\kappa^2} \cos\xi, \tag{A6}$$

$$\text{and } \cos\theta = 1 - 2\kappa^2 \sin^2\xi \tag{A7}$$

so that the expression for τ_b becomes:

$$\tau_b = \frac{2R_0 q}{v_{th}(2\epsilon\gamma)^{1/2}} 4 \int_0^{\pi/2} \frac{\mathrm{d}\xi}{\sqrt{1-\kappa^2 \sin^2 \xi}}. \tag{A8}$$

Using the definitions for complete elliptic integrals of the first and second kind

$$K(\kappa) = \int_0^{\pi/2} \frac{\mathrm{d}\xi}{\sqrt{1-\kappa^2 \sin^2 \xi}},$$

$$E(\kappa) = \int_0^{\pi/2} \mathrm{d}\xi \sqrt{1-\kappa^2 \sin^2 \xi}, \tag{A9}$$

and defining

$$I(\kappa) = \int_0^{\pi/2} \mathrm{d}\xi \, \cos 2\xi \sqrt{1-\kappa^2 \sin^2 \xi}, \tag{A10}$$

we get

$$\tau_b = \frac{2R_0 q}{v_{th}(2\epsilon\gamma)^{1/2}} 4K(\kappa). \tag{A11}$$

The function $I(\kappa)$ can be expressed in terms of elliptic functions. However, we use a 9th order polynomial approximation given by:

$$\begin{aligned} I(x) = & -0.0469408683\, x + 1.35138578\, x^2 \\ & - 10.3802946\, x^3 + 45.5537980\, x^4 - 108.138006\, x^5 \\ & + 142.277853\, x^6 - 97.4188862\, x^7 + 27.1340637\, x^8. \end{aligned} \tag{A12}$$

The forms of these functions are shown in Fig. 12.

The bounce average of any quantity can then be defined as:

$$\langle g(\theta) \rangle_b = \frac{4R_0 q\sqrt{2}}{\tau_b v_{th}(\epsilon\gamma)^{1/2}} \int_0^{\pi/2} \frac{g(\xi)\mathrm{d}\xi}{\sqrt{1-\kappa^2 \sin \xi}}, \tag{A13}$$

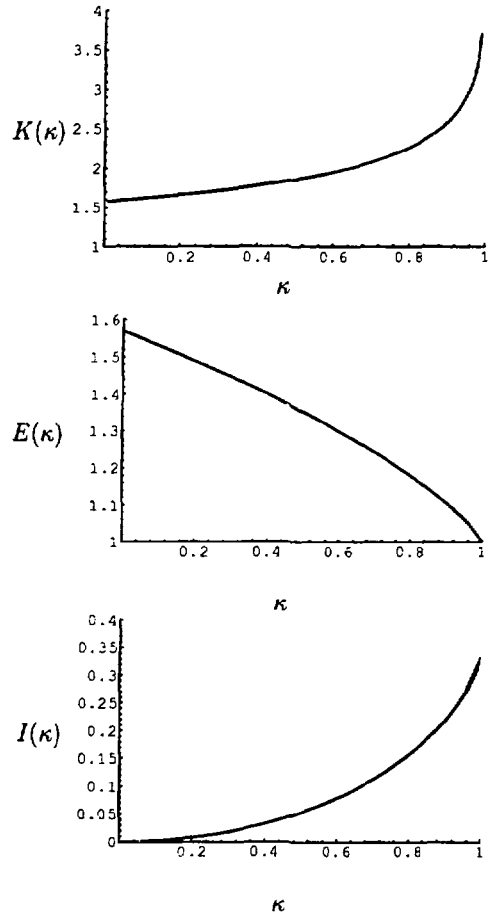

Figure 12: *Plots of the functions $K(\kappa)$, $E(\kappa)$, and $I(\kappa)$. For $I(\kappa)$ both the value obtained by numerical integration and by the polynomial approximation given in Eq. (A12) are plotted.*

or using the expression for τ_b we get:

$$\langle g(\theta)\rangle_b = \frac{1}{K(\kappa)}\int_0^{\pi/2}\frac{g(\xi)\,d\xi}{\sqrt{1-\kappa^2\sin^2\xi}}. \tag{A14}$$

We are interested in calculating $\langle c_\parallel\rangle_b$, $\langle c_\parallel^2\rangle_b$, $\langle\cos\theta\rangle_b$, $\langle\cos^2\theta\rangle_b$, $\langle c_\parallel\rangle_b$, $\langle c_\parallel\cos\theta\rangle_b$, and $c_\parallel^2\cos\theta$. By symmetry, we see that $\langle c_\parallel\rangle_b = 0$, and $\langle c_\parallel\cos\theta\rangle_b = 0$. For the rest of these bounce averages we get:

$$\begin{aligned}\langle\cos\theta\rangle_b &= \frac{1}{K(\kappa)}\int_0^{\pi/2}d\xi\left[2\sqrt{1-\kappa^2\sin^2\xi}-\frac{1}{\sqrt{1-\kappa^2\sin^2\xi}}\right]\\ &= 2\frac{E(\kappa)}{K(\kappa)}-1,\end{aligned} \tag{A15}$$

$$\begin{aligned}\langle c_\parallel^2\rangle_b &= \frac{(\epsilon\gamma)v_{th}^2}{K(\kappa)}\int_0^{\pi/2}\frac{d\xi}{\sqrt{1-\kappa^2\sin^2\xi}}\left[2-2\kappa^2\sin^2\xi-2+2\kappa^2\right]\\ &= (2\epsilon\gamma)v_{th}^2\left[\frac{E(\kappa)}{K(\kappa)}+\kappa^2-1\right],\end{aligned} \tag{A16}$$

$$\begin{aligned}\langle c_\parallel^2\cos\theta\rangle_b &= \frac{(\epsilon\gamma)v_{th}^2}{K(\kappa)}\int_0^{\pi/2}\frac{d\xi}{\sqrt{1-\kappa^2\sin^2\xi}}2\kappa^2\cos 2\xi(1-2\kappa^2\sin^2\xi)\\ &= \frac{(\epsilon\gamma)v_{th}^2}{K(\kappa)}\int_0^{\pi/2}d\xi\left[2\kappa^2\cos 2\xi\sqrt{1-\kappa^2\sin^2\xi}\right.\\ &\quad\left.+\,(2\kappa^2-2)\sqrt{1-\kappa^2\sin^2\xi}+\frac{2-2\kappa^2}{\sqrt{1-\kappa^2\sin^2\xi}}\right]\\ &= (2\epsilon\gamma)v_{th}^2\left[\kappa^2\frac{I(\kappa)}{K(\kappa)}+(2\kappa^2-1)\frac{E(\kappa)}{K(\kappa)}+1-\kappa^2\right],\end{aligned} \tag{A17}$$

and $\langle\cos^2\theta\rangle_b = \dfrac{1}{K(\kappa)}\displaystyle\int_0^{\pi/2}\frac{d\xi}{\sqrt{1-\kappa^2\sin^2\xi}}(1-2\kappa^2\sin^2\xi)^2$

$$= \frac{1}{K(\kappa)} \int_0^{\pi/2} \mathrm{d}\xi \Big[2\kappa^2 \cos 2\xi \sqrt{1-\kappa^2 \sin^2\xi} - 2\kappa^2 \sqrt{1-\kappa^2\sin^2\xi}$$

$$+ \frac{1}{\sqrt{1-\kappa^2\sin^2\xi}} \Big] = 2\kappa^2 \frac{I(\kappa)}{K(\kappa)} - 2\kappa^2 \frac{E(\kappa)}{K(\kappa)} + 1. \tag{A18}$$

A.0.2 Circulating Particles

Similar to the trapped particle calculation, the transit time, τ_t is defined as:

$$\tau_t = \frac{R_0 q}{v_{th}(\epsilon\gamma)^{1/2}} \int_{-\pi}^{\pi} \frac{\mathrm{d}\theta}{\sqrt{2\kappa^2 - 1 + \cos\theta}}. \tag{A19}$$

Introducing the variable $\xi = \theta/2$ with $\mathrm{d}\theta = 2\mathrm{d}\xi$, we get:

$$\tau_t = \frac{4R_0 q}{v_{th}(\epsilon\gamma)^{1/2}} \int_0^{\pi/2} \frac{\mathrm{d}\xi}{\sqrt{2}\kappa\sqrt{1-\kappa^{-2}\sin^2\xi}} = \frac{R_0 q}{v_{th}(2\epsilon\gamma)^{1/2}} \frac{4}{\kappa K(\kappa^{-1})}. \tag{A20}$$

Then, the transit average of any quantity $g(\theta)$ can be defined as:

$$\langle g(\theta)\rangle_t = \frac{1}{K(\kappa^{-1})} \int_0^{\pi/2} \frac{g(\xi)\mathrm{d}\xi}{\sqrt{1-\kappa^{-2}\sin^2\xi}}. \tag{A21}$$

The various quantities of interest will then be given by:

$$\langle \cos\theta\rangle_t = \frac{1}{K(\kappa^{-1})} \int_0^{\pi/2} \frac{\mathrm{d}\xi}{\sqrt{1-\kappa^{-2}\sin^2\xi}} \left[2\kappa^2(1-\kappa^{-2}\sin^2\xi) + 1 - 2\kappa^2 \right]$$

$$= 2\kappa^2 \frac{E(\kappa^{-1})}{K(\kappa^{-1})} + (1-2\kappa^2), \tag{A22}$$

$$\langle c_\parallel^2\rangle_t = \frac{v_{th}^2(\epsilon\gamma)}{K(\kappa^{-1})} \int_0^{\pi/2} \frac{\mathrm{d}\xi}{\sqrt{1-\kappa^{-2}\sin^2\xi}} 2\kappa^2(1-\kappa^{-2}\sin^2\xi)$$

$$= (2\epsilon\gamma) v_{th}^2 \kappa^2 \frac{E(\kappa^{-1})}{K(\kappa^{-1})}, \tag{A23}$$

$$\langle c_\parallel^2 \cos\theta\rangle_t = \frac{(\epsilon\gamma)v_{th}^2}{K(\kappa^{-1})} \int_0^{\pi/2} \mathrm{d}\xi\, 2\kappa^2 \cos 2\xi \sqrt{1-\kappa^{-2}\sin^2\xi}$$

$$= (2\epsilon\gamma)v_{th}^2\kappa^2\frac{I(\kappa^{-1})}{K(\kappa^{-1})}, \tag{A24}$$

$$\langle\cos^2\theta\rangle_t = \frac{1}{K(\kappa^{-1})}\int_0^{\pi/2}\frac{\mathrm{d}\xi\,\cos^2 2\xi}{\sqrt{1-\kappa^{-2}\sin^2\xi}}$$

$$= \frac{1}{K(\kappa^{-1})}\int_0^{\pi/2}\frac{\mathrm{d}\xi}{\sqrt{1-\kappa^{-2}\sin^2\xi}}\left[2\kappa^2(1-\kappa^{-2}\sin^2\xi)\cos 2\xi\right.$$

$$\left. + \; 2\kappa^2(1-2\kappa^2)(1-\kappa^{-2}\sin^2\xi) + (1-2\kappa^2)^2\right]$$

$$= 2\kappa^2\frac{I(\kappa^{-1})}{K(\kappa^{-1})} + 2\kappa^2(1-2\kappa^2)\frac{E(\kappa^{-1})}{K(\kappa^{-1})} + (1-2\kappa^2)^2, \tag{A25}$$

and $\quad \langle c_\parallel\rangle_t = \dfrac{\sigma_\parallel v_{th}(\epsilon\gamma)^{1/2}}{K(\kappa^{-1})}\displaystyle\int_0^{\pi/2}\frac{\mathrm{d}\xi\,\sqrt{2}\kappa\,\cos\xi}{\sqrt{1-\kappa^{-2}\sin^2\xi}}$

$$= \sigma_\parallel(2\epsilon\gamma)^{1/2}v_{th}\,\frac{\kappa\pi}{2K(\kappa^{-1})}. \tag{A26}$$

Appendix B. Integration Limits

The presence of the electrostatic trapping term requires the velocity space integrals for trapped and transit particles to be handled carefully. An inspection of the expression for parallel velocity in Eq. (28) and μ will show that the velocity space integral, in terms of the guiding center variables can be expressed as:

$$\int 2\pi c_\perp \mathrm{d}c_\perp\,\mathrm{d}c_\parallel = \sum_{\sigma_\parallel}\int_{-\epsilon g\cos\theta/h}^{\infty}\mathrm{d}E'$$

$$\times\int_0^{(hE'+\epsilon g\cos\theta)/B_0}\frac{\mathrm{d}\mu B_0\pi\sqrt{2}}{h(\theta)M^{3/2}\sqrt{E'-\mu B_0/h(\theta)+\epsilon g\cos\theta/h(\theta)}}. \tag{B1}$$

In terms of the dimensionless variables introduced in Sec. II.A this will be given by:

$$\int 2\pi c_\perp dc_\perp dc_\parallel = \frac{\pi v_{th}^3}{2} \sum_{\sigma_\parallel} \int_{-\epsilon\bar{g}\cos\theta/h}^{\infty} d\bar{E} \int_0^{h\bar{E}+\epsilon\bar{g}\cos\theta} \frac{d\bar{\mu}}{h(\theta)\sqrt{\bar{E} - \bar{\mu}/h(\theta) + \epsilon\bar{g}\cos\theta/h(\theta)}}. \tag{B2}$$

Or, using the definition of Λ from Sec. II.A it can be written as:

$$\int 2\pi c_\perp dc_\perp dc_\parallel = \frac{\pi v_{th}^3}{2} \sum_{\sigma_\parallel} \int_{-\epsilon\bar{g}\cos\theta/h}^{\infty} d\bar{E} \int_{\bar{g}/(\bar{E}+\bar{g})}^{h} \frac{d\Lambda(\bar{E}+\bar{g})^{1/2}}{h\sqrt{1 - \Lambda/h(\theta)}}. \tag{B3}$$

With regard to separating the trapped and circulating particle integrals it is important to note that for $\bar{E} < \epsilon\bar{g}/(1-\epsilon)$, the lower limit of $\bar{\mu}$ integration will not depend on $\bar{E}$. Hence the trapped particle integral, in terms of $\bar{E}$, and $\bar{\mu}$ will consist of two parts in the form:

$$\int_{-\epsilon\bar{g}\cos\theta/h(\theta)}^{\epsilon\bar{g}/(1-\epsilon)} d\bar{E} \int_0^{h(\theta)\bar{E}+\epsilon\bar{g}\cos\theta} d\bar{\mu} + \int_{\epsilon\bar{g}/(1-\epsilon)}^{\infty} d\bar{E} \int_{(1-\epsilon)\bar{E}-\epsilon\bar{g}}^{h(\theta)\bar{E}+\epsilon\bar{g}\cos\theta} d\bar{\mu}. \tag{B4}$$

Let us now treat the trapped and circulating particle integrations separately.

Appendix C. Trapped particle integration

In terms of $\bar{E}$ and Λ, the trapped particle integral will be of the form:

$$\int_{-\bar{g}\epsilon\cos\theta/h}^{\epsilon\bar{g}/(1-\epsilon)} d\bar{E} \int_{\bar{g}/(\bar{E}+\bar{g})}^{h} d\Lambda + \int_{\epsilon\bar{g}/(1-\epsilon)}^{\infty} d\bar{E} \int_{1-\epsilon}^{h} d\Lambda. \tag{C1}$$

Since we are eventually interested in taking the Fourier transform, we will operate with $\int_{-\pi}^{\pi} d\theta$ on the velocity integrals. The energy integral on the right does not have θ dependent bounds, thus we only have to consider the one on the left. We observe that the limits of $\bar{E}$ integration are even in θ and considering $\int_0^{\pi} d\theta$ will be sufficient. Since the lower limit of $\bar{E}$ integration is a one to one function of θ, it can be inverted to yield:

$$\int_{-\epsilon\bar{g}/(1+\epsilon)}^{\epsilon\bar{g}/(1-\epsilon)} d\bar{E} \int_0^{\cos^{-1}(-\bar{E}/[\epsilon(\bar{g}+\bar{E})])} d\theta \int_{\bar{g}/(\bar{E}+\bar{g})}^{h} d\Lambda. \tag{C2}$$

We again see that only the upper bound of the Λ integral has a dependence on θ. Hence, inverting the limits we get:

$$\int_{-\epsilon\bar{g}/(1+\epsilon)}^{\epsilon\bar{g}/(1-\epsilon)} \mathrm{d}\bar{E} \int_{\bar{g}/(\bar{E}+\bar{g})}^{1+\epsilon} \mathrm{d}\Lambda \int_0^{\theta_0(\Lambda)} \mathrm{d}\theta. \tag{C3}$$

Switching the order of the $\bar{E}$ and Λ integrations and adding the contribution of the integral on the right in Eq. (C1) we have:

$$\int_{1-\epsilon}^{1+\epsilon} \mathrm{d}\Lambda \int_{\bar{g}(1-\Lambda)/\Lambda}^{\infty} \mathrm{d}\bar{E} \int_{-\theta_0(\Lambda)}^{\theta_0(\Lambda)} \mathrm{d}\theta. \tag{C4}$$

We can now transform the energy variable $\bar{E}$ to get rid of Λ-dependent bounds such that:

$$\bar{E} = Y + \frac{\bar{g}}{\Lambda} - \bar{g}. \tag{C5}$$

The integral over trapped particles can then be expressed as:

$$\int_{1-\epsilon}^{1+\epsilon} \mathrm{d}\Lambda \int_0^{\infty} \mathrm{d}Y \int_{-\theta_0(\Lambda)}^{\theta_0(\Lambda)} \mathrm{d}\theta. \tag{C6}$$

The exact expression for the trapped particle velocity space integral including the Fourier transform will then be given by:

$$\frac{1}{2\pi} \int_{-\pi}^{\pi} \mathrm{d}\theta \int_{\text{trapped}} 2\pi c_\perp \mathrm{d}c_\perp \mathrm{d}c_\parallel = \frac{v_{th}^3}{4} \sum_{\sigma_\parallel} \int_{1-\epsilon}^{1+\epsilon} \mathrm{d}\Lambda \int_0^{\infty} \mathrm{d}Y \int_{-\theta_0(\Lambda)}^{\theta_0(\Lambda)} \mathrm{d}\theta \frac{(Y+\bar{g}/\Lambda)^{1/2}}{\sqrt{1-\Lambda/h(\theta)}}. \tag{C7}$$

For orbit integrals the expression for $c_\parallel$ will be given by:

$$c_\parallel = \sigma_\parallel v_{th} \gamma^{1/2} \sqrt{1 - \frac{\Lambda}{h(\theta)}}, \tag{C8}$$

with

$$\gamma = Y + \frac{\bar{g}}{\Lambda}. \tag{C9}$$

Appendix D. Transit Particle integration

For transit particles we have no problem taking the θ integral inside because none of the integration limits depend on θ. In terms of $\bar{E}$ and $\bar{\mu}$ the circulating particle integral will be of the form:

$$\int_{\epsilon\bar{g}/(1-\epsilon)}^{\infty} \mathrm{d}\bar{E} \int_{0}^{(1-\epsilon)\bar{E}-\epsilon\bar{g}} \mathrm{d}\bar{\mu}, \tag{D1}$$

and using $\bar{E}$ and Λ we get:

$$\int_{\epsilon\bar{g}/(1-\epsilon)}^{\infty} \mathrm{d}\bar{E} \int_{\bar{g}/(\bar{E}+\bar{g})}^{(1-\epsilon)} \mathrm{d}\Lambda. \tag{D2}$$

We can define $\bar{E}' = \bar{E} - \epsilon\bar{g}/(1-\epsilon)$ and change the order of integration for $\bar{E}'$ and Λ to get:

$$\int_{0}^{1-\epsilon} \mathrm{d}\Lambda \int_{\bar{g}/\Lambda-\bar{g}/(1-\epsilon)}^{\infty} \mathrm{d}\bar{E}'. \tag{D3}$$

To remove the Λ-dependence on the energy integral we use

$$\bar{E} = Y + \frac{\bar{g}}{\Lambda} - \bar{g}. \tag{D4}$$

Finally, the circulating particle velocity space integration with the Fourier transform is given by:

$$\frac{1}{2\pi}\int_{-\pi}^{\pi} \mathrm{d}\theta \int_{\text{transit}} 2\pi c_{\perp}\, \mathrm{d}c_{\perp}\, \mathrm{d}c_{\parallel} = \frac{v_{th}^3}{4} \sum_{\sigma_{\parallel}} \int_{0}^{1-\epsilon} \mathrm{d}\Lambda \int_{0}^{\infty} \mathrm{d}Y \int_{-\pi}^{\pi} \mathrm{d}\theta \frac{(Y+\bar{g}/\Lambda)^{1/2}}{\sqrt{1-\Lambda/h(\theta)}}. \tag{D5}$$

Then the expression for parallel velocity will be given by:

$$c_{\parallel} = \sigma_{\parallel} v_{th} \gamma^{1/2} \sqrt{1 - \frac{\Lambda}{h(\theta)}}, \tag{D6}$$

where

$$\gamma = Y + \frac{\bar{g}}{\Lambda}. \tag{D7}$$

References

[1]R. J. LaHaye, L. L. Lao, T. H. Osborne, and C. L. Rettig, Bull. Am. Phys. Soc. **39**, 1646 (1994).

[2]R. J. Fonck, R. D. Durst, H. Evensen, J. S. Kim, and S. F. Paul, Bull. Am. Phys. Soc. **39**, 1699 (1994).

[3]B. B. Kadomtsev and O. P. Pogutse, Sov. Phys. JETP **24**, 1178 (1967).

[4]W. M. Tang, Nuclear Fusion **18**, 1089 (1978).

[5]M. N. Rosenbluth, D. W. Ross, and D. P. Kostomarov, Nuclear Fusion **12**, 3 (1972).

[6]R. Marchand, *Two-Dimensional Eigenmode Analyis of the Trapped-Ion Instability*, PhD thesis, Princeton University Princeton, NJ 08543, 1979.

[7]R. Marchand, W. M. Tang, and G. Rewoldt, Phys. Fluids **23**, 980 (1980).

[8]M. Artun and W. M. Tang, Phys. Plasmas **1**, 2682 (1994).

[9]P. J. Catto, I. B. Bernstein, and M. Tessarotto, Phys. Fluids **30**, 2784 (1987).

[10]R. D. Hazeltine, Phys. Fluids B **1**. 2031 (1989).

[11]K. H. Burrell, 1994, Private Communication.

[12]R. J. Fonck, 1994, Private Communication.

[13]W. M. Tang and G. Rewoldt, Phys. Fluids B **5**, 2451 (1993).

EXTERNAL DISTRIBUTION IN ADDITION TO UC-420

Dr. F. Paoloni, Univ. of Wollongong, AUSTRALIA
Prof. R.C. Cross, Univ. of Sydney, AUSTRALIA
Plasma Research Lab., Australian Nat. Univ., AUSTRALIA
Prof. I.R. Jones, Flinders Univ, AUSTRALIA
Prof. F. Cap, Inst. for Theoretical Physics, AUSTRIA
Prof. M. Heindler, Institut für Theoretische Physik, AUSTRIA
Prof. M. Goossens, Astronomisch Instituut, BELGIUM
Ecole Royale Militaire, Lab. de Phy. Plasmas, BELGIUM
Commission-European, DG. XII-Fusion Prog., BELGIUM
Prof. R. Boucique, Rijksuniversiteit Gent, BELGIUM
Dr. P.H. Sakanaka, Instituto Fisica, BRAZIL
Prof. Dr. I.C. Nascimento, Instituto Fisica, Sao Paulo, BRAZIL
Instituto Nacional De Pesquisas Espaciais-INPE, BRAZIL
Documents Office, Atomic Energy of Canada Ltd., CANADA
Ms. M. Morin, CCFM/Tokamak de Varennes, CANADA
Dr. M.P. Bachynski, MPB Technologies, Inc., CANADA
Dr. H.M. Skarsgard, Univ. of Saskatchewan, CANADA
Prof. J. Teichmann, Univ. of Montreal, CANADA
Prof. S.R. Sreenivasan, Univ. of Calgary, CANADA
Prof. R. Marchand, INRS-Energie et Materiaux, CANADA
Dr. R. Bolton, Centre canadien de fusion magnétique, CANADA
Dr. C.R. James,, Univ. of Alberta, CANADA
Dr. P. Lukác, Komenského Universzita, CZECHO-SLOVAKIA
The Librarian, Culham Laboratory, ENGLAND
Library, R61, Rutherford Appleton Laboratory, ENGLAND
Mrs. S.A. Hutchinson, JET Library, ENGLAND
Dr. S.C. Sharma, Univ. of South Pacific, FIJI ISLANDS
P. Mähönen, Univ. of Helsinki, FINLAND
Prof. M.N. Bussac, Ecole Polytechnique,, FRANCE
C. Mouttet, Lab. de Physique des Milieux Ionisés, FRANCE
J. Radet, CEN/CADARACHE - Bat 506, FRANCE
Prof. E. Economou, Univ. of Crete, GREECE
Ms. C. Rinni, Univ. of Ioannina, GREECE
Preprint Library, Hungarian Academy of Sci., HUNGARY
Dr. B. DasGupta, Saha Inst. of Nuclear Physics, INDIA
Dr. P. Kaw, Inst. for Plasma Research, INDIA
Dr. P. Rosenau, Israel Inst. of Technology, ISRAEL
Librarian, International Center for Theo Physics, ITALY
Miss C. De Palo, Associazione EURATOM-ENEA , ITALY
Dr. G. Grosso, Istituto di Fisica del Plasma, ITALY
Prof. G. Rostangni, Istituto Gas Ionizzati Del Cnr, ITALY
Dr. H. Yamato, Toshiba Res & Devel Center, JAPAN
Prof. I. Kawakami, Hiroshima Univ., JAPAN
Prof. K. Nishikawa, Hiroshima Univ., JAPAN
Librarian, Naka Fusion Research Establishment, JAERI, JAPAN
Director, Japan Atomic Energy Research Inst., JAPAN
Prof. S. Itoh, Kyushu Univ., JAPAN
Research Info. Ctr., National Instit. for Fusion Science, JAPAN
Prof. S. Tanaka, Kyoto Univ., JAPAN
Library, Kyoto Univ., JAPAN
Prof. N. Inoue, Univ. of Tokyo, JAPAN
Secretary, Plasma Section, Electrotechnical Lab., JAPAN
Dr. O. Mitarai, Kumamoto Inst. of Technology, JAPAN
Dr. G.S. Lee, Korea Basic Sci. Ctr., KOREA
J. Hyeon-Sook, Korea Atomic Energy Research Inst., KOREA
D.I. Choi, The Korea Adv. Inst. of Sci. & Tech., KOREA
Leandro Melendez Lugo, Inst. Nacl. de Inves. Nucl, MEXICO
Prof. B.S. Liley, Univ. of Waikato, NEW ZEALAND
Inst of Physics, Chinese Acad Sci PEOPLE'S REP. OF CHINA
Library, Inst. of Plasma Physics, PEOPLE'S REP. OF CHINA
Tsinghua Univ. Library, PEOPLE'S REPUBLIC OF CHINA
Z. Li, S.W. Inst Physics, PEOPLE'S REPUBLIC OF CHINA
Prof. J.A.C. Cabral, Instituto Superior Tecnico, PORTUGAL
Prof. M.A. Hellberg, Univ. of Natal, S. AFRICA
Prof. D.E. Kim, Pohang Inst. of Sci. & Tech., SO. KOREA
Prof. C.I.E.M.A.T, Fusion Division Library, SPAIN
Dr. L. Stenflo, Univ. of UMEA, SWEDEN
Library, Royal Inst. of Technology, SWEDEN
Prof. H. Wilhelmson, Chalmers Univ. of Tech., SWEDEN
Centre Phys. Des Plasmas, Ecole Polytech, SWITZERLAND
Bibliotheek, Inst. Voor Plasma-Fysica, THE NETHERLANDS
Asst. Prof. Dr. S. Cakir, Middle East Tech. Univ., TURKEY
Dr. V.A. Glukhikh,Sci. Res. Inst. Electrophys.l Apparatus, USSR
Dr. D.D. Ryutov, Siberian Branch of Academy of Sci., USSR
Dr. G.A. Eliseev, I.V. Kurchatov Inst., USSR
Librarian, The Ukr.SSR Academy of Sciences, USSR
Dr. L.M. Kovrizhnykh, Inst. of General Physics, USSR
Kernforschungsanlage GmbH, Zentralbibliothek, W. GERMANY
Bibliothek, Inst. Für Plasmaforschung, W. GERMANY
Prof. K. Schindler, Ruhr-Universität Bochum, W. GERMANY
Dr. F. Wagner, (ASDEX), Max-Planck-Institut, W. GERMANY
Librarian, Max-Planck-Institut, W. GERMANY